A Theoretical and Empirical Investigation into the Equivalence of Graph Neural Networks and the Weisfeiler-Leman Algorithm

From the faculty of Mathematics, Physics, and Computer Science approved for the purpose of obtaining the academic degree of Bachelor of Sciences.

Eric Tillmann Bill

Supervision:
Prof. Dr. rer. nat. Christopher Morris

Informatik 6
RWTH Aachen University

July 13, 2023

Acknowledgements

Luis, Christopher und HPC RWTH

Contents

1. Introduction

This work aims to shed light on the representations learned by Graph Neural Networks. In this section, we will discuss the prevalence of graphs and the crucial role GNNs play in analyzing them. We will delve into the methods we use to gain insights and highlight the significance of our approach. Lastly, we will provide an overview of the structure of this work.

1.1. Motivation

Graphs are ubiquitous in various fields of life. Despite not always being explicitly identified as such, the graph data model's flexibility and simplicity make it an effective tool for modeling a diverse range of data. Examples of graph modeling applications include unexpected instances, such as modeling text or images as a graph, as well as more complex instances like chemical molecules, citation networks, or connectivity encodings of the World Wide Web Morris et al. [2020], Scarselli et al. [2009].

Although machine learning has achieved remarkable success with image classification (e.g., Zoph et al. [2018], He et al. [2016]) and text generation (e.g., Radford et al. [2019], Brown et al. [2020]) in the last decade, the lack of a significant breakthrough in machine learning for graphs can be attributed to the graph data model's inherent flexibility and simplicity. While, for example, an image classifier constrains its input data to be a grid-like image or a text generator expects its input to be a linear sequence of words, machine learning models working on graphs cannot leverage any constraints on the format or size of their input graphs without limiting their generality.

To put this flexibility of the graph data model into perspective and give an idea of how ubiquitous graphs are in various fields, we refer back to the examples of image classifiers and text generators and demonstrate how seemingly natural the graph data model can encode their input data. For example, images can be encoded by a graph, such that each pixel of the image corresponds to a node in the graph holding its color value, and each node is connected to its neighboring pixel nodes. Similarly, for sequential data like text files, one can encode a directed graph where each word in this file is represented as a node with the word as a feature and connected outgoingly to the next following word. See Figure 1 for an illustrative example of these encodings.

In recent years, a significant amount of research has been conducted to investigate Graph Neural Networks (GNNs). Among the most promising approaches are those utilizing the message-passing architecture, which was introduced by Scarselli et al. [2009] and Gilmer et al. [2017]. Empirically, this framework has demonstrated strong performance across various applications Kipf and Welling [2017], Hamilton et al. [2017], Xu et al. [2019]. However, its expressiveness is limited, as has been proved by the works of Morris et al. [2019], as well as Xu et al. [2019]. These works establish a connection to the commonly used Weisfeiler-Leman[1] algorithm (1-WL), originally proposed by Weisfeiler and Leman [1968] as a simple heuristic for the graph isomorphism problem. In particular, it has been proven that a GNN based on the message-passing architecture can, at most, be as good as the 1-WL algorithm in distinguishing non-isomorphic graphs. Furthermore, the 1-WL method demonstrates numerous similarities with the fundamental workings of the GNN architecture. It is, therefore, commonly believed

[1] Based on https://www.iti.zcu.cz/wl2018/pdf/leman.pdf, we will use the spelling "Leman" here, as requested by A. Leman, the co-inventor of the algorithm.

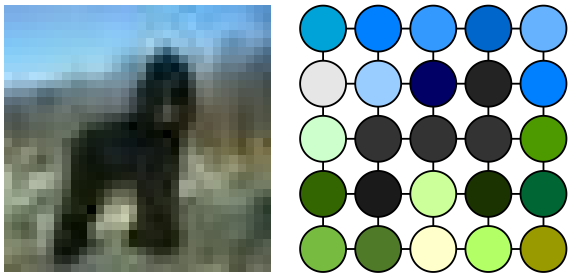

(a) Example for an image of a dog.[2]

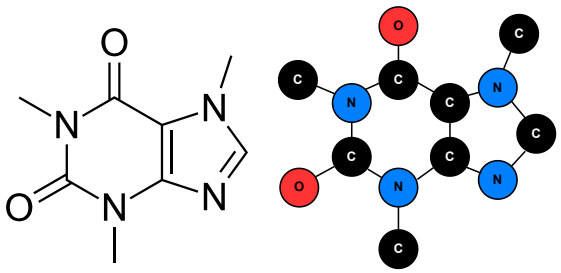

(b) Example for the molecule caffeine.[3]

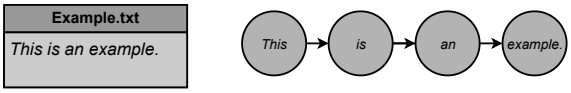

(c) Example for a text file.

Figure 1.: Here are some examples of how graphs can be used to encode information in a variety of domains. Please note that these examples are just a sample, and in actual practice, more detailed encodings are usually utilized to capture additional information.[4]

that both methods are, to some extent, equivalent in their capacity to capture information in a graph.

OUTLOOOK WHAT IS THE MOTIVATION NOW?

Footnotes are wrong!

more colorful and downscaled example :(

1.2. Research Questions & Contributions

Test

1.3. Methology

In this work, we introduce a novel framework, which we coined "1-WL+NN," which involves applying the 1-WL algorithm to an input graph and further processing the resulting information using a feedforward neural network. Thereby, we obtain a trainable framework suited for all kinds of graph-related tasks, such as graph classification, node regression, and more. We will prove later on that both frameworks, 1-WL+NN and GNN, are theoretically equivalent, such that each function computed by a 1-WL+NN model can also be computed by a GNN model and vice versa. With this framework in hand, we can investigate the representations learned by a GNN.

The interesting property of this framework compared to GNNs, which is also the original idea that inspired this work, is the fundamental difference in how both frameworks learn and optimize themselves when applied to a specific task. Take, for example, an arbitrary classification task. While the first part of a 1-WL+NN model starts by applying the 1-WL algorithm to its input graph and retrieves a highly informative representation of this graph, the second part, the learnable feedforward neural network, must find common patterns in this very detailed representation that coincides with the classes of the task, such that the model makes good predictions. In comparison, while a GNN is theoretically as expressive as the 1-WL

[2]The image is from the CIFAR-10 collection made available by Krizhevsky et al. [2009].
[3]The illustration of the skeletal formula of caffeine is taken from https://commons.wikimedia.org.
[4]All graphics were created using the free open source platform https://www.draw.io.

algorithm, we imagine that such a model first leans to find common patterns as early as possible in the input graph and will drop irrelevant information as soon as possible before making a class prediction.

To put both learning behaviors into perspective: while the 1-WL+NN is given a maximally informative representation and needs to find the important information to make a good prediction, a GNN works the other way around and needs to learn how it constructs its own informative representation of the input graph and how to leverage this information for making a prediction. Therefore, we expect 1-WL+NN models to perform sufficiently well on their training data but expect poor generalization capabilities due to the too-informative representations computed by the 1-WL algorithm. In contrast, we expect more promising generalization capabilities of GNNs in comparison since they optimize for the best representation of their input graphs and might leverage this information more efficiently.

We will use this novel framework and various empirical experiments to compare both frameworks on multiple datasets to establish a deeper understanding of the representations learned by GNNs.

1.4. Outline

For the ease of readability, we split this work into two parts. The first part investigates and establishes the theoretical equivalence between the frameworks of 1-WL+NN and GNNs. In contrast, the second part discusses our different experiments and their empirical results and insights into GNNs.

In detail, this work starts with Section 2, where we discuss related work, milestones in GNNs over the past decade, essential properties of the 1-WL algorithm, and a subset of interesting connections between GNNs and the 1-WL algorithm. Afterward, we will start with Part I, which begins with Section 3. Here, we will introduce formal definitions for both frameworks, as well as a set of notations we will use throughout the theoretical part. Afterward, in Section 4, we will introduce four theorems that each present a connection between both frameworks and combined prove the equivalence of both frameworks. Finally, we will prove each theorem individually after another in corresponding subsections.

The second part will deal with ...

2. Background and Related Work

In this section, we will briefly introduce the foundation of our research by explaining the origins of the two frameworks, mentioning important recent advances, and providing a brief overview of the connections between them.

2.1. Weisfeiler-Leman Algorithm

The (1-dimensional) Weisfeiler-Leman algorithm (1-WL), proposed by Weisfeiler and Leman [1968], was initially designed as a simple heuristic for the *graph isomorphism problem*, but due to its interesting properties, its simplicity, and its good performance, the 1-WL algorithm gained a lot of attention from researchers across many fields. One of the most noticeable properties is that the algorithm color codes the nodes of the input graph in such a way that in each iteration, each color encodes a learned local substructure.

It works by coloring all nodes in each iteration the same color that fulfills two properties: 1. the nodes already share the same color, and 2. each color appears equally often in the set of the nodes direct neighbors. The algorithm continues as long as the number of colors changes in each iteration. For determining whether two graphs are non-isomorphic, the heuristic is applied to both graphs simultaneously. It concludes that the graphs are non-isomorphic as soon as the number of occurrences of a color differs between them. We present a more formal definition of the algorithm in the following part in Section 3.3.

Since the *graph isomorphism problem* is difficult to solve due to the best known complete algorithm only running in deterministic quasipolynomial time (Babai [2016]), the 1-WL algorithm, running in deterministic polynomial time, cannot solve the problem completely. Moreover, Cai et al. [1992] constructed counterexamples of non-isomorphic graphs that the heuristic fails to distinguish, e.g., see Figure 3. However, following the work of Babai and Kucera [1979], this simple heuristic is still quite powerful and has a very low probability of failing to distinguish non-isomorphic graphs when both graphs are uniformly chosen at random as the number of nodes tends to infinity.

To overcome the limited expressiveness of the 1-WL algorithm, it has been generalized to the k-dimensional Weisfeiler-Leman algorithm (k-WL) by Babai [1979, 2016], as well as Immerman and Lander [1990][5]. This version works with k-tuples over the k-ary Cartesian product of the set of nodes. Interestingly, this created a hierarchy for the expressiveness of determining non-isomorphism, such that for all $k \in \mathbb{N}$ there exists a pair of non-isomorphic graphs that can be distinguished by the $(k+1)$-WL but not by the k-WL (Cai et al. [1992]).

2.2. Graph Neural Networks

The idea of leveraging machine learning techniques, previously proven effective in various domains, for graph-related tasks has been a well-established topic in the literature for the past decades. However, researchers faced challenges in effectively adapting these techniques to graphs of diverse sizes and complexities in the early stages. Notably, the works by Sperduti and Starita [1997], Scarselli et al. [2008], and Micheli [2009] were the first prominent examples of successful applications in this regard.

However, it was not until the emergence of more advanced models that the scientific community truly recognized the significance and potential of Graph Neural Networks (GNNs). Noteworthy among these advancements were the work of Duvenaud et al. [2015], who introduced a differentiable approach for generating unique fingerprints of arbitrary graphs, as well as Li et al. [2015], who applied gated recurrent units to capture graphs of various sizes, while Atwood and Towsley [2016] utilized diffusional convolutions for the same purpose. Of particular significance, however, were the contributions of Bruna et al. [2013], Defferrard et al. [2016] and Kipf and Welling [2017], which extended the concept of convolution from its traditional application on images to the domain of arbitrary graphs.

After the early success of these GNN models, Gilmer et al. [2017] introduced a unified architecture for GNNs. The authors observed a recurring pattern in how information is exchanged and processed among many of these works, including many mentioned in the paragraph above. Leveraging these observations, Gilmer et al. [2017] devised the message-passing architecture as a generalized framework for GNNs. Models using this architecture can

[5] In Babai [2016] on page 27, László Babai explains that he, together with Rudolf Mathon, first introduced this algorithm in 1979. He adds that the work of Immerman and Lander [1990] introduced this algorithm independently of him.

be referred to as Message-Passing-Neural-Network (MPNN); however, throughout this thesis, we will use the term GNN and MPNN interchangeably, as the focus of this thesis is solely on the message-passing architecture. This architecture uses the input graph as its basis for computation and computes new node features for the graph in each layer. The computation of each new node feature involves aggregating all the features of the neighboring nodes and the node's own feature. After applying each layer of a GNN model, a representation of the entire graph is obtained by applying a pooling function (e.g. Ying et al. [2018]). This representation is then further processed by common machine learning techniques like a multilayer perceptron for the final output. We will present a more formal definition of this architecture in the following part in Section 3.5; however, important to note is that the information exchange in the graph across nodes is limited to a one-hop neighbor per layer.

With this general framework and the empirical success of some models using this message-passing architecture, the question of how expressive models based on this architecture can be gained a lot of attention in the scientific community. Many papers immediately established connections to the 1-WL algorithm, among the most prominent being Morris et al. [2019] and Xu et al. [2019]. These connections seem natural, as both methods share similar properties in terms of how they process graph data. Most strikingly, both methods never change the graph structurally since they only compute new node features in each iteration. Moreover, both methods use a one-hop neighborhood aggregation as the basis for computing the new node feature. Following this intuition, Morris et al. [2019], as well as Xu et al. [2019], showed that the expressiveness of GNNs is upper-bounded by the 1-WL in terms of distinguishing non-isomorphic graphs. Moreover, Morris et al. [2019] proposed a new k-GNN architecture that operates over the set of subgraphs of size k. Interestingly, Geerts [2020] has shown that the proposed hierarchy over $k \in \mathbb{N}$ is equivalent to the k-WL hierarchy in terms of its ability to distinguish non-isomorphic graphs, i.e., if there is a k-GNN that can distinguish two non-isomorphic graphs, it is equivalent to say that the k-WL algorithm can also distinguish these graphs.

Although there are other modifications of the message-passing architecture besides the theoretical concept of k-GNN to increase the expressiveness of GNNs in terms of distinguishing non-isomorphism, e.g., using node identifiers Vignac et al. [2020], adding random node features Sato et al. [2021], Abboud et al. [2020], adding directed flows Beaini et al. [2021] and many more. Relatively few works have been published that attempt to understand the representation learned from a standard GNN.

Notable works include Nikolentzos et al. [2023b], where the author, in addition to the normal learning process, optimized GNNs to preserve a notion of distance in their representation and examined the effectiveness of GNNs in utilizing such representations. However, their insights can only be applied to these specially trained GNN models and not be generalized. In another publication, Nikolentzos et al. [2023a] presented mathematical proof and empirical confirmation showing how much structural information is encoded by modern GNN models. Their research highlights that GNN models like DGCNN (Zhang et al. [2018]) and GAT (Veličković et al. [2017]) encode all nodes with the same feature vector, while in contrast, models like GCN (Kipf and Welling [2017]) and GIN (Xu et al. [2019]) encode nodes after k layers of message-passing with features that relate with the number of walks of length k over the input graph form each node, disregarding the local structure within the nodes are contained.

Part I.

Theoretical Equivalence

This part of the thesis focuses on the equivalence between 1-WL+NN and GNN. We will begin by providing a preliminary section that formalizes all the concepts used in the proof and introduces a general notation. Afterward, we will dedicate a separate section to present and prove three theorems. These theorems combined conclude the equivalence.

3. Preliminaries

This section will introduce and formalizes all concepts used throughout the proof and the rest of the thesis. We start with general notations, introduce a general graph definition, and familiarize the reader with the Weisfeiler-Leman algorithm. We will introduce each framework independently, first the 1-WL+NN and then GNN. In the end, we will briefly introduce important properties of collections of functions computed by both methods.

3.1. General Notation

Let $\mathbb{N}$ denote the set of natural numbers such that $\mathbb{N} := \{0, 1, 2, \ldots\}$. By $[n]$, we denote the set $\{0, \ldots, n\} \subset \mathbb{N}$ for each $n \in \mathbb{N}$. Further, with $\{\!\{\ldots\}\!\}$, we denote a multiset formally defined as a 2-tuple (X, m), where X is a set of all unique elements and $m : X \to \mathbb{N}_{\geq 1}$ a mapping that maps each element in X to the number of its occurrences in the multiset.

3.2. Graphs

We will briefly introduce a formal definition for graphs and coloring on graphs. Starting with the definition of a graph.

Definition 1 (Graph)**.** A graph G is defined as a 3-tuple denoted by $G \coloneqq (V, E, l)$. This tuple consists of a set of nodes $V \subset \mathbb{N}$, a set of edges $E \subseteq V \times V$, and a labeling function $l : M \to \Sigma$. The domain M of the labeling function can be either V, $V \cup E$, or E, and the codomain Σ is an alphabet with $\Sigma \subseteq \mathbb{N}^k$, where $k \in \mathbb{N}$ is arbitrary. In the context of this thesis, the assigned values by the labeling function are referred to as either labels or features, depending on the dimension of Σ. In detail, if $k = 1$, we usually refer to the values as labels, otherwise as features. Additionally, the set of all graphs is denoted by $\mathcal{G}$.

Furthermore, a graph G can be either directed or undirected based on the definition of its set of edges E. If $E \subseteq \{(v, u) \mid v, u \in V\}$, it represents a directed graph, whereas if $E \subseteq \{(v, u) \mid v, u \in V, v \neq u\}$ such that for every $(v, u) \in E$ there exists $(u, v) \in E$, it defines an undirected graph. Additionally, for ease of notation, we will use $V(G)$ and $E(G)$ to denote the set of nodes and the set of edges of G, respectively, as well as l_G to denote the label function of G. Further, with $\mathcal{N}(v)$ for $v \in V(G)$ we denote the set of neighbors of v defined as $\mathcal{N}(v) \coloneqq \{u \mid (u, v) \in E(G)\}$, and with $d(v)$ for $v \in V(G)$ the degree of node v, defined as $d(v) := |\mathcal{N}(v)|$.

We continue with the definition of a graph coloring.

Definition 2 (Graph Coloring)**.** A coloring of a Graph G is a function $C : V(G) \to \mathbb{N}$ that assigns each node in the graph a color (here, a positive integer). Further, a coloring C induces a partition $\mathcal{P}$ on the set of nodes, for which we define C^{-1} being the function that maps each color $c \in \mathbb{N}$ to its class of nodes with $C^{-1}(c) = \{v \in V(G) \mid C(v) = c\}$. In addition, we define $h_{G,C}$ as the histogram of graph G with coloring C that maps every color in the image of C under $V(G)$ to the number of occurrences. In detail, $\forall c \in \mathbb{N} : h_{G,C}(c) \coloneqq |\{v \in V(G) \mid C(v) = c\}| = |C^{-1}(c)|$.

Permutation-invariance and -equivariance

We use S_n to denote the symmetric group over the elements $[n]$ for any $n \in \mathbb{N}$. S_n consists of all permutations over these elements. Let G be a graph with $V(G) = [n]$, applying a permutation $\pi \in S_n$ on G, is defined as $G_\pi \coloneqq \pi \cdot G$ where $V(G_\pi) = \{\pi(0), \ldots, \pi(n)\}$ and $E(G_\pi) = \{(\pi(v), \pi(u)) \mid (v, u) \in E(G)\}$. We will now introduce two key concepts for classifying functions on graphs.

Definition 3 (Permutation Invariant)**.** Let $f : \mathcal{G} \to \mathcal{Y}$ be an arbitrary function, then f is *permutation-invariant* if and only if for all $G \in \mathcal{G}$, where $n_G \coloneqq \mid V(G) \mid$ and for every $\pi \in S_{n_G}$: $f(G) = f(\pi \cdot G)$.

Definition 4 (Permuation Equivariant)**.** Let $f : \mathcal{G} \to \mathcal{Y}$ be an arbitrary function, then f is *permuation-equivariant* if and only if for all $G \in \mathcal{G}$, where $n_G \coloneqq \mid V(G) \mid$ and for every $\pi \in S_{n_G}$: $f(G) = \pi^{-1} \cdot f(\pi \cdot G)$.

3.3. Weisfeiler and Leman Algorithm

The Weisfeiler-Leman algorithm consists of two main parts: the coloring algorithm and the graph isomorphism test. We will introduce each part individually and present some implications afterward.

The Weisfeiler-Leman Graph Coloring Algorithm

The 1-WL algorithm computes a node coloring of its input graph in each iteration. In detail, a color is assigned to each node based on the colors of its neighbors and its own current color. The algorithm continues until convergence is reached, resulting in the final coloring of the graph. We will now formally define this procedure and provide an illustrative example in Figure 2.

Definition 5 (1-WL Algorithm)**.** Let $G = (V, E, l)$ be a labeled graph. In each iteration i, the 1-WL algorithm computes a node coloring $C_i : V(G) \to \mathbb{N}$. In the initial iteration $i = 0$, the coloring is set to $C_0 = l$ if l exists. Otherwise, for all $v \in V(G) : C_0(v) = c$ with $c \in \mathbb{N}$ being an arbitrary but fixed constant. For $i > 0$, the algorithm assigns a color to $v \in V(G)$ as follows:

$$C_i(v) = \mathsf{RELABEL}(C_{i-1}(v),\ \{\!\{C_{i-1}(u) \mid u \in \mathcal{N}(v)\}\!\}),$$

where RELABEL injectively maps the above pair to a unique, previously not used, color. The algorithm terminates when the number of colors between two iterations does not change, meaning the algorithm terminates after iteration i if the following condition is satisfied:

$$\forall v, w \in V(G) : C_i(v) = C_i(w) \iff C_{i+1}(v) = C_{i+1}(w).$$

Upon terminating we define $C_\infty \coloneqq C_i$ as the stable coloring, such that $\text{1-WL}(G) \coloneqq C_\infty$.

The colorings computed in each iteration always converge to the final one, such that the algorithm always terminates. In more detail, Grohe [2017] showed that it always holds after at most $|V(G)|$ iterations. For an illustration of this algorithm, see Figure 2. Moreover, based on the work of Paige and Tarjan [1987] about efficient refinement strategies, Cardon and Crochemore [1982] proved that the stable coloring C_∞ can be computed in time $\mathcal{O}(|V(G)| + |E(G)| \cdot \log |V(G)|)$.

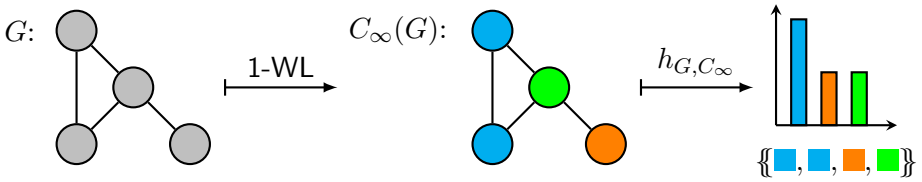

Figure 2.: An example of the final coloring computed by applying the 1-WL algorithm on the graph G. The graph G consists of 4 nodes with all their labels being set to the same color.

It is important to understand that since the algorithm was originally developed as a simple heuristic for the *graph isomorphism problem*, which is an inherently discrete problem, the 1-WL algorithm in its simplest form, as we presented it here, does only work on graphs with discrete, one-dimensional node labels. Although it is quite easy to adapt the algorithm to respect discrete edge labels of a graph by using them as weights in the neighborhood aggregation (Shervashidze et al. [2011]), modifying its definition to work with continuous graph features is more complex. Numerous proposed modifications have been put forward to address this integration in the literature, such as those discussed by Morris et al. [2016]. However, note that this particular topic will not be further investigated in this thesis, although its mention holds value for the following section.

The Weisfeiler-Leman Graph Isomorphism Test

The isomorphism test uses the 1-WL coloring algorithm and is defined as follows.

Definition 6 (1-WL Isomorphism Test)**.** To determine if two graphs $G, H \in \mathcal{G}$ are non-isomorphic ($G \ncong H$), one applies the 1-WL coloring algorithm on both graphs "in parallel" and checks after each iteration if the occurrences of each color are equal, else the algorithm would terminate and conclude non-isomorphic. Formally, the algorithm concludes non-isomorphic in iteration i if there exists a color c such that:

$$|\{v \in V(G) \mid C_i(v) = c\}| \neq |\{v \in V(H) \mid C_i(v) = c\}|.$$

Note that this test is only sound and not complete for the *graph isomorphism problem*. Counterexamples can be easily constructed where the algorithm fails to distinguish non-isomorphic graphs. See Figure 3 for a straightforward example of where this test fails that was discovered and proven by Cai et al. [1992].

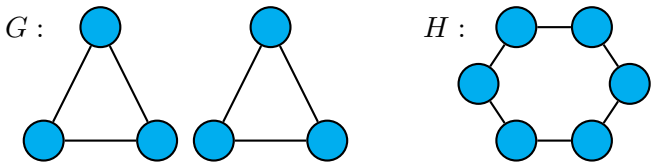

Figure 3.: This is an example of two graphs G and H that are non-isomorphic but cannot be distinguished by the 1-WL isomorphism test.

Implications of the 1-WL Algorithm

One intriguing implication of the 1-WL algorithm and its isomorphism test is that, due to it not being complete for solving the *graph isomorphism problem*, it gives rise to a related but weaker relation than the isomorphism relation ($\simeq$). We define this relation as follows.

Definition 7 (1-WL Relation)**.** Let $\mathcal{X} \subseteq \mathcal{G}$. For any graphs $G, H \in \mathcal{X}$ we will denote $G \simeq_{1\text{WL}} H$ if the 1-WL isomorphism test can not distinguish both graphs. Note that due to the soundness of this algorithm, if $G \not\simeq_{1\text{WL}} H$, we always can conclude that $G \not\simeq H$.

The $\simeq_{1\text{WL}}$ relation can further be classified as an equivalence relation, as it is reflexive, symmetric and transitive. With this, we introduce a notation of its equivalence classes. Let $\mathcal{X} \subseteq \mathcal{G}$ and $G \in \mathcal{X}$, then we denote with $\mathcal{X}/\simeq_{1\text{WL}}(G) := \{G' \in \mathcal{X} \mid G \simeq_{1\text{WL}} G'\}$ its equivalence class.

Similarly, we define the notion 1-WL-Discriminating for collections of permutation invariant functions.

Definition 8 (1-WL-Discriminating)**.** Let $\mathcal{X} \subseteq \mathcal{G}$. Further, let $\mathcal{C}$ be a collection of permutation invariant functions from $\mathcal{X}$ to $\mathbb{R}$. We say $\mathcal{C}$ is 1-WL-Discriminating if for all graphs $G_1, G_2 \in \mathcal{X}$ for which the 1-WL isomorphism test concludes non-isomorphic ($G_1 \not\simeq_{1\text{WL}} G_2$), there exists a function $h \in \mathcal{C}$ such that $h(G_1) \neq h(G_2)$.

3.4. 1-WL+NN

As the previous section shows, the 1-WL algorithm is quite powerful in identifying a graph's substructures and distinguishing non-isomorphic graph pairs. With the 1-WL+NN framework, we define functions that utilize this structural information to derive application-specific insights.

Definition 9 (1-WL+NN)**.** A 1-WL+NN model consists of three components that are applied sequentially to its input: 1. the 1-WL algorithm, 2. an encoding function f_{enc} operating on graph colorings, and 3. an arbitrary multilayer perceptron MLP. In detail, a 1-WL+NN model computes the function $\mathcal{B}$, that is defined as follows:

$$\mathcal{B} : \mathcal{G} \to \mathbb{R}^k,\ G \mapsto \text{MLP} \circ f_{\text{enc}}(\{\!\{\text{1-WL}(G)(v) \mid v \in V(G)\}\!\}),$$

where "1-WL(G)" is the coloring computed by the 1-WL algorithm when applied on G, and $k \in \mathbb{N}$ is an arbitrary constant. For a better understanding and an illustrative explanation, see Figure 4.

It is worth noting that this definition can be easily adjusted to accommodate node or edge-related tasks by applying the encoding function f_{enc} and the multilayer perceptron MLP elementwise to the colors of the multiset. However, for the purposes of this thesis, we will not delve into these variations, as our main focus will be on graph-wide tasks such as graph classification or regression, which possess greater theoretical interest and are more prevalent in most datasets. Furthermore, all the theoretical findings presented in this thesis can also be applied to 1-WL+NN models designed for node or edge tasks.

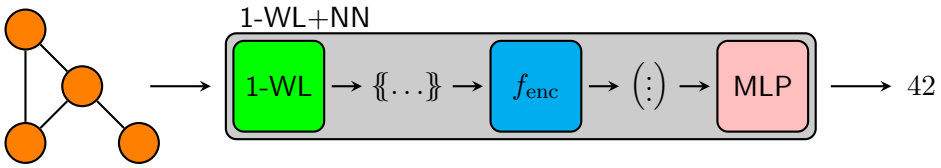

Figure 4.: This simplified illustration explains the components that make up a 1-WL+NN model and how each one processes the input further. In detail, the model takes the graph on the left as input and first applies the 1-WL algorithm, thereby obtaining a multiset of the colors assigned by the algorithm. Then the encoding function f_{enc} is applied, resulting in a fixed-sized vector that is further processed by the multilayer perceptron MLP. The output of the MLP is then propagated as the 1-WL+NN models output, here the number 42.

3.5. Graph Neural Networks (Message-Passing)

A Graph Neural Network (GNN) is a composition of multiple layers, where each layer computes a new feature for each node and edge. Each GNN layer thus technically obtains a new graph structurally identical to the previous one but contains new feature information. After an input graph has been passed through all layers, a final readout function is applied that pools all graph features and derives a task-related output. With this, it is possible to apply a GNN to every graph, regardless of its size, as the "computation" will only take place on the nodes and edges of the graph.

Note that in the following, we will restrict the definition only to consider node features; however, one can easily extend it to include edge features as well.

Definition 10 (Graph Neural Network)**.** Let $G = (V, E, l)$ be an arbitrary graph. A GNN is a composition of multiple layers and a final readout function where each layer t is represented by a function $f^{(t)}$. The initial layer at $t = 0$ is a functioning of the format $f^{(0)} : V(G) \to \mathbb{R}^{1\times d}$ that is consistent with l and translates all labels into a vector representation. In contrast, for every $t > 0$, $f^{(t)}$ is recursively defined as:

$$f^{(t)}(v) = f^{(t)}_{\text{merge}}(f^{(t-1)}(v),\ f^{(t)}_{\text{agg}}(\{\!\{f^{(t-1)}(w) \mid w \in \mathcal{N}(v)\}\!\})),$$

where $f^{(t)}_{\text{merge}}$ is an arbitrary function that maps the aforementioned tuple to a vector, effectively "merging" them, while $f^{(t)}_{\text{agg}}$ is an arbitrary function that maps the multiset to a vector, effectively "aggregating" it.

The readout function, referred to as Readout, is applied after the input graph has been passed subsequently through all layers and is defined as follows:

$$\text{Readout}(\{\!\{f^{(t)}(v) \mid v \in V(G)\}\!\}).$$

This function pools the information from every node feature, processes it, and calculates a fixed-sized output vector for the entire graph.

In summary, a GNN model will compute the function $\mathcal{A}$ defined as follows:

$$\mathcal{A} : \mathcal{G} \to \mathbb{R}^k,\ G \mapsto \text{Readout}(\{\!\{f^{(T)}(v) \mid v \in V(G)\}\!\}),$$

where T is the number of layer of the GNN, and $k \in \mathbb{N}$ an arbitrary constant. To enable end-to-end training of a GNN, it is essential that all its components are differentiable. Therefore,

we require all $f_{\text{merge}}^{(t)}$ and $f_{\text{agg}}^{(t)}$ functions for all $t \in [T]$, along with the final Readout function, to be differentiable.

Note that, due to our definition of the "aggregation" and the "readout" function to operate over multisets, both functions are permutation invariant by definition. With this, we can conclude that the total composition $\mathcal{A}$ is permutation invariant, and with similar reasoning, it is also differentiable. This property enables us to train $\mathcal{A}$ like any other machine learning method in an end-to-end fashion, regardless of the underlying encoding used for graphs. Furthermore, GNNs following this definition are regarded as Message-Passing-Neural-Network (MPNN). This designation stems from each node exchanging information with its direct neighbors in each layer. As a result, information during the processing of a graph is propagated by passing many messages across the graph; thus, these layers are also referred to as *message-passing* layers. As outlined in the introduction to this thesis, we will solely focus on GNNs utilizing the *message-passing* architecture. Therefore we will use the term GNN and MPNN interchangeably throughout this thesis. The definition and notation used here are inspired by Morris et al. [2019] and Xu et al. [2019].

To bridge the gap from the theoretical definition to practical instances of the definition, we will now introduce three distinct GNN architectures. Specifically, we will explore the Graph Attention Network (GAT) developed by Veličković et al. [2017], Graph Convolutional Network (GCN) proposed by Kipf and Welling [2017], and the Graph Isomorphism Network (GIN) introduced by Xu et al. [2019]. These architectures will serve as empirical baselines in Part II. Additionally, we will also elaborate on the reasons for this choice of models in Part II in Section 5.2. We listed the definitions of the *message-passing* layers of each model in Table 1.

Table 1.: Overview of the construction of the *message-passing* layers and their respective learnable parameters by popular GNN model. This format is inspired by Nikolentzos et al. [2023a].

Model	**Message-Passing Layer Definition**	**Learnable Parameters**
GAT	$f^{(t)}(v) = \sigma\Big(\sum_{u \in \mathcal{N}(v)} \alpha_{vu} \cdot W^{(t)} \cdot f^{(t-1)}(u)\Big)$ with $\alpha_{vu} = \frac{\exp\big(\text{LeakyReLU}\big(\vec{a}^T \cdot \mathsf{concat}[W^{(t)} f^{(t-1)}(v),\ W^{(t)} f^{(t-1)}(u)]\big)\big)}{\sum_{k \in \mathcal{N}(v)} \exp\big(\text{LeakyReLU}\big(\vec{a}^T \cdot \mathsf{concat}[W^{(t)} f^{(t-1)}(v),\ W^{(t)} f^{(t-1)}(k)]\big)\big)}$	$\vec{a}, W^{(t)}$
GCN	$f^{(t)}(v) = \text{ReLU}\Big(\sum_{u \in \mathcal{N}(v) \cup \{v\}} \frac{W^{(t)}}{\sqrt{(1+d(v)) \cdot (1+d(u))}} f^{(t-1)}(u)\Big)$	$W^{(t)}$
GIN	$f^{(t)}(v) = \mathsf{MLP}^{(t)}\Big((1+\epsilon^{(t)}) \cdot f^{(t-1)}(v) + \sum_{u \in \mathcal{N}(v)} f^{(t-1)}(u)\Big)$	$\epsilon^{(t)}, \mathsf{MLP}^{(t)}$

Commonly employed Readout functions in this context often involve straightforward pooling techniques like elementwise summation, mean calculation, or maximum extraction. These pooling operations are typically followed by a multilayer perceptron, which performs additional processing on the aggregated information. Although more sophisticated pooling operations exist, such as Set2Set developed by Vinyals et al. [2015], Xu et al. [2019] showed that given the correct configuration, the elementwise summation pooling function combined with a following multilayer perceptron suffices to create a GNN that is as expressive as the 1-WL algorithm in distinguishing non-isomorphism.

4. Theoretical Connection

This section is the main part of our theoretical investigation of the two frameworks 1-WL+NN and GNN. We will present three intriguing theorems, which will be proven separately afterward. In detail, the first two theorems will establish an equivalence between the two frameworks when the input set of graphs is finite. While the last theorem will take this a step further and demonstrate how powerful the 1-WL algorithm is by establishing a connection between 1-WL+NN and GNN for continuous functions.

In the first two theorems, we focus on a finite collection of graphs, which we denote by $\mathcal{X}$ with $\mathcal{X} \subset \mathcal{G}$.

Theorem 11 (Finite Case: "GNN $\subseteq$ 1-WL+NN")**.** Let $\mathcal{C}$ be a collection of functions from $\mathcal{X}$ to $\mathbb{R}$ computable by GNNs, then $\mathcal{C}$ is also computable by 1-WL+NN.

Theorem 12 (Finite Case: "1-WL+NN $\subseteq$ GNN")**.** Let $\mathcal{C}$ be a collection of functions from $\mathcal{X}$ to $\mathbb{R}$ computable by 1-WL+NN, then $\mathcal{C}$ is also computable by GNNs.

With these two theorems, the equivalence between both frameworks follows. Specifically, every function computed by 1-WL+NN working over any arbitrary, but finite $\mathcal{X} \subset \mathcal{G}$ is also computable by a GNN, and vice versa. As we move towards the empirical evaluation in Part II, it is evident that if we test a 1-WL+NN model on any of the benchmark datasets, it can achieve theoretically the same level of performance as a GNN model. Notice that we did not leverage any constraints on the encoding of graphs throughout the first two theorems and their corresponding proves but instead kept it general.

Having established a connection between the two frameworks on a finite subset of graphs, we wanted to further demonstrate the expressive power of the 1-WL algorithm and in particular of collections of functions that are 1-WL-Discriminating by investigating a connection between the two frameworks for continuous feature spaces and continuous functions. However, since the *graph isomorphism problem* is an inherently discrete problem, the 1-WL algorithm, as outlined in Section 3.4, is only defined as a discrete and discontinuous function operating on discrete colors, such that extending the definition of the 1-WL algorithm to a continuous function working over continuous values is not very trivial and, to our knowledge, has not yet been widely investigated. Therefore, we assume in the proof and the following theorem that such a continuous version of the 1-WL algorithm exists.

We define the set of graphs with continuous labels using the following definition.

Definition 13. Let X be a compact subset of $\mathbb{R}$ including 0. We decode graphs with n nodes as a matrix $G \in X^{n \times n}$, where $G_{i,i}$ decodes the label of node i for $i \in [n]$, and $G_{i,j}$ with $i \neq j \in [n]$ decodes an edge from node i to j and a corresponding edge features. Furthermore, we say that there is an edge between node i and j if and only if $G_{i,j} \neq 0$. Additionally, if G encodes an undirected graph, G is a symmetric matrix. For simplicity, we denote $\mathcal{X} \coloneqq X^{n \times n}$ throughout the next theorem.

Then the following theorem can be derived.

Theorem 14 (Continuous Case: "GNN $\subseteq$ 1-WL+NN")**.** Let $\mathcal{C}$ be a collection of continuous functions from $\mathcal{X}$ to $\mathbb{R}$ computable by 1-WL+NN. If $\mathcal{C}$ is 1-WL-Discriminating, then there exists a collection of functions $\mathcal{C}'$ computable by 1-WL+NN that is GNN-Approximating.

The notion of a collection of functions capable of approximating any GNN function is defined as follows.

Definition 15 (GNN-Approximating)**.** Let $\mathcal{C}$ be a collection of permutation invariant functions from $\mathcal{X}$ to $\mathbb{R}$. We say $\mathcal{C}$ is GNN-Approximating if for all permutation-invariant functions $\mathcal{A}$ computed by a GNN, and for all $\epsilon \in \mathbb{R}$ with $\epsilon > 0$, there exists $h_{\mathcal{A},\epsilon} \in \mathcal{C}$ such that $\|\mathcal{A} - h_{\mathcal{A},\epsilon}\|_\infty \coloneqq \sup_{G \in \mathcal{X}} |\mathcal{A}(G) - h_{\mathcal{A},\epsilon}(G)| < \epsilon$

Since we only wanted to show the expressive power of 1-WL-Discriminating and made the major assumption of the existence of a continuous 1-WL algorithm, we have included the proof of Theorem 14 in the Appendix in subsection 1.2.

By putting all theorems into perspective, we can conclude that the ability 1-WL-Discriminating is very powerful, so we can assume that 1-WL+NN is sufficiently expressive for the upcoming empirical part.

4.1. Proof of Theorem 11: "GNN $\subseteq$ 1-WL+NN"

We will prove Theorem 11 by introducing a couple of small lemmas, which combined prove the theorem. In detail, in Lemma 16, we show the existence of a collection computed by 1-WL+NN that is 1-WL-Discriminating. In Lemmas 17 to 19 we derive properties of 1-WL+NN functions we will use throughout Lemmas 20 to 22 with which we prove the theorem. We took great inspiration for Lemmas 20 to 22 from the proof presented in section 3.1 in the work of Chen et al. [2019].

Lemma 16. There exists a collection $\mathcal{C}$ of functions from $\mathcal{X}$ to $\mathbb{R}$ computable by 1-WL+NN that is 1-WL-Discriminating.

Proof. We define f_c for $c \in \mathbb{N}$ as the encoding function that returns the number of nodes colored as c. With this, we can construct the collection of functions C as follows:

$$C := \{\mathcal{B}_c : \mathcal{X} \to \mathbb{R},\ G \mapsto \mathsf{MLP}_{\text{id}} \circ f_c(\{\!\{\text{1-WL}(G)(v) \mid v \in V(G)\}\!\}) \mid c \in \mathbb{N}\},$$

where MLP_{id} is a dummy multilayer perceptron that returns its input. Since every function $\mathcal{B}_c \in C$ is composed of the 1-WL algorithm, an encoding function, and a multilayer perceptron, each function is computable by 1-WL+NN, and consequently also the whole collection.

Proof of correctness: Let $G_1, G_2 \in \mathcal{X}$ with $G_1 \not\simeq_{\text{1WL}} G_2$. Further, let C_1, C_2 be the final colorings computed by the 1-WL algorithm when applied on G_1, G_2 respectively. Due to $G_1 \not\simeq_{\text{1WL}} G_2$, there exists a color $c \in \mathbb{N}$ such that $h_{G_1,C_1}(c) \neq h_{G_2,C_2}(c)$. Such that $\mathcal{B}_c \in C$ exists with $\mathcal{B}_c(G_1) \neq \mathcal{B}_c(G_2)$. □

Lemma 17 (1-WL+NN Equivalence)**.** Let $\mathcal{B}$ be a function over $\mathcal{X}$ computable by 1-WL+NN, then for every pair of graphs $G_1, G_2 \in \mathcal{X}$: if $G_1 \simeq_{\text{1WL}} G_2$ than $\mathcal{B}(G_1) = \mathcal{B}(G_2)$.

Proof. Let $\mathcal{B}$ be an arbitrary function over $\mathcal{X}$ computable by 1-WL+NN, then $\mathcal{B}$ is composed as follows: $\mathcal{B}(\cdot) = \mathsf{MLP} \circ f_{\text{enc}}\{\!\{\text{1-WL}(\cdot)(v) \mid v \in V(\cdot)\}\!\}$. Further, let $G_1, G_2 \in \mathcal{X}$ be arbitrary graphs with $G_1 \simeq_{\text{1WL}} G_2$, then by definition of the relation $\simeq_{\text{1WL}}$ we know that 1-WL(G_1) = 1-WL(G_2). With this, the equivalence follows immediately. □

Lemma 18 (1-WL+NN Permuation Invariance)**.** Let $\mathcal{B}$ be a function over $\mathcal{X}$ computable by 1-WL+NN, then $\mathcal{B}$ is permutation invariant.

Proof. Let $G_1, G_2 \in \mathcal{X}$ be arbitrary graphs with $G_1 \simeq G_2$ and $\mathcal{B}$ an arbitrary function computable by 1-WL+NN. Since the 1-WL algorithm is sound, we know that $G_1 \simeq G_2$ implies $G_1 \simeq_{\text{1WL}} G_2$. Using Lemma 17, we can therefore conclude that: $\mathcal{B}(G_1) = \mathcal{B}(G_2)$. □

Lemma 19 (1-WL+NN Composition)**.** Let $\mathcal{C}$ be a collection of functions computable by 1-WL+NN. Further, let $h_1, \dots h_n \in \mathcal{C}$ and $\mathsf{MLP}^\bullet$ an multilayer perceptron, than the function $\mathcal{B}$ composed of $\mathcal{B}(\cdot) \coloneqq \mathsf{MLP}^\bullet(h_1(\cdot), \dots, h_n(\cdot))$ is also computable by 1-WL+NN.

Proof Sketch. Assume the above and let $f_1, \dots, f_n$ be the encoding functions, as well as $\mathsf{MLP}_1, \dots, \mathsf{MLP}_n$ be the multilayer perceptrons used by $h_1, \dots, h_n$ respectively. The idea of this proof is that we construct an encoding function f^* that "duplicates" its input and applies each encoding function f_i individually. We also construct a multilayer perceptron MLP^* that takes in the output of f^* and simulates all $\mathsf{MLP}_1, \dots, \mathsf{MLP}_n$ simultaneously. Afterward, the given $\mathsf{MLP}^\bullet$ will be applied on the concatenation of the output of all MLP_i's. See Figure 5 for a sketch of the proof idea. For the complete proof, please refer to the Appendix in subsection 1.1.

$$G \xmapsto{\text{1-WL}} \begin{array}{c} M_G \coloneqq \\ \{\!\{\text{1-WL}(G)(v) \mid v \in V(G)\}\!\} \end{array} \xmapsto{f^*} \begin{bmatrix} f_1(M_G) \\ \vdots \\ f_n(M_G) \end{bmatrix} \xmapsto{\text{MLP}^*} \text{MLP}^\bullet\Big(\begin{bmatrix} \text{MLP}_1(f_1(M_G)) \\ \vdots \\ \text{MLP}_n(f_n(M_G)) \end{bmatrix} \Big)$$

Figure 5.: The proof idea for Lemma 19, how the constructed functions f^* and MLP^* will work on input $G \in \mathcal{X}$. Here we denote with M_G the multiset of colors of the nodes of G after applying the 1-WL algorithm.

Lemma 20. Let $\mathcal{C}$ be a collection of functions from $\mathcal{X}$ to $\mathbb{R}$ computable by 1-WL+NN that is 1-WL-Discriminating. Then for all $G^* \in \mathcal{X}$, there exists a function h_{G^*} from $\mathcal{X}$ to $\mathbb{R}$ computable by 1-WL+NN, such that for all $G \in \mathcal{X} : h_{G^*}(G) = 0$, if and only if, $G \simeq_{1\text{WL}} G^*$.

Proof. Assume the above. For any $G_1, G_2 \in \mathcal{X}$ with $G_1 \not\simeq_{1\text{WL}} G_2$, let $h_{G_1,G_2} \in \mathcal{C}$ be the function distinguishing them, with $h_{G_1,G_2}(G_1) \neq h_{G_1,G_2}(G_2)$. We define the function $\overline{h}_{G_1,G_2}$ working over $\mathcal{X}$ as follows:

$$\begin{aligned} \overline{h}_{G_1,G_2}(\cdot) &= |h_{G_1,G_2}(\cdot) - h_{G_1,G_2}(G_1)| \\ &= \max(h_{G_1,G_2}(\cdot) - h_{G_1,G_2}(G_1),\ 0) + \max(h_{G_1,G_2}(G_1) - h_{G_1,G_2}(\cdot),\ 0) \\ &= \text{ReLU}(h_{G_1,G_2}(\cdot) - h_{G_1,G_2}(G_1)) + \text{ReLU}(h_{G_1,G_2}(G_1) - h_{G_1,G_2}(\cdot)) \end{aligned} \tag{0.1}$$

Note, that in the equations above "$h_{G_1,G_2}(G_1)$" is a fixed constant and the resulting function $\overline{h}_{G_1,G_2}$ is non-negative. Let $G_1 \in \mathcal{X}$ now be fixed, we will construct the function h_{G_1} with the desired properties as follows:

$$h_{G_1}(\cdot) = \sum_{G_2 \in \mathcal{X},\ G_1 \not\simeq_{1\text{WL}} G_2} \overline{h}_{G_1,G_2}(\cdot). \tag{0.2}$$

Since $\mathcal{X}$ is finite, the sum is finite and therefore well-defined. Next, we will prove that for a fixed graph $G_1 \in \mathcal{X}$, the function h_{G_1} is correct on input $G \in \mathcal{X}$:

1. If $G_1 \simeq_{1\text{WL}} G$, then for every function $\overline{h}_{G_1,G_2}$ of the sum with $G_1 \not\simeq_{1\text{WL}} G_2$, we know, using Lemma 17, that $\overline{h}_{G_1,G_2}(G)$ is equal to $\overline{h}_{G_1,G_2}(G_1)$ which is by definition 0, such that $h_{G_1}(G) = 0$.
2. If $G_1 \not\simeq_{1\text{WL}} G$, then $\overline{h}_{G_1,G}(G)$ is a summand of the overall sum, and since $\overline{h}_{G_1,G}(G) > 0$, we can conclude $h_{G_1}(G) > 0$ due to the non-negativity of each function $\overline{h}_{G_1,G_2}$.

Using Lemma 19, we can conclude that for any $G \in \mathcal{X}$, h_G is computable by 1-WL+NN, as we can encode Equation 0.2 via a multilayer perceptron where the factor "$h_{G_1,G_2}(G_1)$" of Equation 0.1 is just a constant. □

Lemma 21. Let $\mathcal{C}$ be a collection of functions from $\mathcal{X}$ to $\mathbb{R}$ computable by 1-WL+NN so that for all $G^* \in \mathcal{X}$, there exists $h_{G^*} \in \mathcal{C}$ satisfying $h_{G^*}(G) = 0$ if and only if $G \simeq_{1\text{WL}} G^*$, for all $G \in \mathcal{X}$. Then for every $G^* \in \mathcal{X}$, there exists a function φ_{G^*} computable by 1-WL+NN such that for all $G \in \mathcal{X}$: $\varphi_{G^*}(G) = \mathbb{1}_{G \simeq_{1\text{WL}} G^*}$.

Proof. Assuming the above. Due to $\mathcal{X}$ being finite, we can define for every graph G^* the constant:

$$\delta_{G^*} \coloneqq \frac{1}{2} \min_{G \in \mathcal{X},\ G \not\simeq_{1\text{WL}} G^*} |h_{G^*}(G)| > 0.$$

With this constant, we can use a so-called "bump" function working from $\mathbb{R}$ to $\mathbb{R}$ that is similar to the indicator function. We define this function for parameter $a \in \mathbb{R}$ with $a > 0$ as:

$$\begin{aligned} \psi_a(x) &\coloneqq \max(\frac{x}{a} - 1,\ 0) + \max(\frac{x}{a} + 1,\ 0) - 2 \cdot \max(\frac{x}{a},\ 0) \\ &= \text{ReLU}(\frac{x}{a} - 1) + \text{ReLU}(\frac{x}{a} + 1) - 2 \cdot \text{ReLU}(\frac{x}{a}) \end{aligned} \tag{0.3}$$

The interesting property of ψ_a is that it maps every value x to 0, except when x is being drawn from the interval $(-a, a)$. In particular, it maps x to 1 if and only if x is equal to 0. See Figure 6 for a plot of the relevant part of this function with exemplary values for a.

We use these properties to define for every graph $G^* \in \mathcal{X}$ the function $\varphi_{G^*}(\cdot) \coloneqq \psi_{\delta_{G^*}}(h_{G^*}(\cdot))$. We will quickly demonstrate that this function is equal to the indicator function, for this let G^* be fixed and G, an arbitrary graph from $\mathcal{X}$, the input:

1. If $G \simeq_{1\text{WL}} G^*$, then $h_{G^*}(G) = 0$ resulting in $\varphi_{G^*}(G) = \psi_{\delta_{G^*}}(0) = 1$.
2. If $G \not\simeq_{1\text{WL}} G^*$ then $h_{G^*}(G) \neq 0$, such that $|h_{G^*}(G)| > \delta_{G^*}$ so that $h_{G^*}(G) \notin (-\delta_{G^*}, \delta_{G^*})$ resulting in $\varphi_{G^*}(G) = 0$.

Note that we can encode φ_{G^*} using Equation 0.3 via a multilayer perceptron, where δ_{G^*} is a constant. With Lemma 19 we can therefore conclude that φ_{G^*} is computable by 1-WL+NN for every graph $G^* \in \mathcal{X}$. □

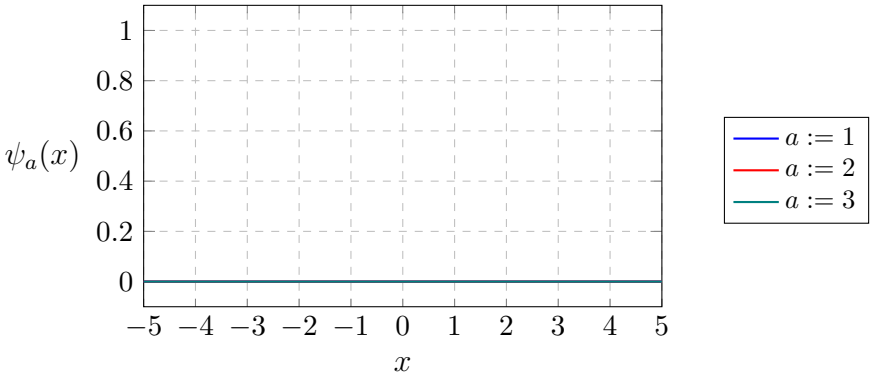

Figure 6.: Illustration of the so-called "bump" function $\psi_a(x)$ used in the proof of Lemma 21 with different exemplary values for a.

Lemma 22. Let $\mathcal{C}$ be a collection of functions from $\mathcal{X}$ to $\mathbb{R}$ computable by 1-WL+NN such that for all $G^* \in \mathcal{X}$, there exists $\varphi_{G^*} \in \mathcal{C}$ satisfying $\forall G \in \mathcal{X} : \varphi_{G^*}(G) = \mathbb{1}_{G \simeq_{1\text{WL}} G^*}$. Then every function computable by a GNN is also computable by 1-WL+NN.

Proof. Assume the above. For any function $\mathcal{A}$ computed by a GNN that works over $\mathcal{X}$ to $\mathbb{R}$, we show that it can be decomposed as follows for any $G \in \mathcal{X}$ as input:

$$\begin{aligned}\mathcal{A}(G) &= \Big(\frac{1}{|\mathcal{X}/\!\simeq_{1\text{WL}}(G)|} \sum_{G^* \in \mathcal{X}} \mathbb{1}_{G \simeq_{1\text{WL}} G^*} \Big) \cdot \mathcal{A}(G) \\ &= \frac{1}{|\mathcal{X}/\!\simeq_{1\text{WL}}(G)|} \sum_{G^* \in \mathcal{X}} \mathcal{A}(G^*) \cdot \mathbb{1}_{G \simeq_{1\text{WL}} G^*} \\ &= \sum_{G^* \in \mathcal{X}} \frac{\mathcal{A}(G^*)}{|\mathcal{X}/\!\simeq_{1\text{WL}}(G^*)|} \cdot \varphi_{G^*}(G) \end{aligned} \tag{0.4}$$

where we denote with $\mathcal{X}/\!\simeq_{1\text{WL}}(G^*)$ the set of all graphs G over $\mathcal{X}$ that are equivalent to G^* according to the $\simeq_{1\text{WL}}$ relation.

Since $\mathcal{A}$ is permutation-invariant and GNNs are, at most, as good as the 1-WL algorithm in distinguishing non-isomorphic graphs, we can use the fact that for every pair of graphs $G, H \in \mathcal{X}$ with $G \simeq_{1\text{WL}} H$: $\mathcal{A}(G) = \mathcal{A}(H)$. Therefore, we can decompose $\mathcal{A}$ as indicated in Equation 0.4 and encode it using a multilayer perceptron where $\frac{\mathcal{A}(G^*)}{|\mathcal{X}/\!\simeq_{1\text{WL}}(G^*)|}$ is a constant, and $\varphi_{G^*} \in \mathcal{C}$ encodes the indicator function. Combined with the Lemma 19, we can conclude that $\mathcal{A}$ is computable by 1-WL+NN. Important to note, we can only do this since $\mathcal{X}$ is finite, making the overall sum finite and the cardinality of $\mathcal{X}/\!\simeq_{1\text{WL}}(G^*)$ well-defined for all graphs. □

4.2. Proof of Theorem 12: "1-WL+NN $\subseteq$ GNN"

In this section we will prove the converse direction. We start with Lemma 23, where we introduce an upper bound that we will use in Lemma 24 to show that there exists a collection of GNN-computable functions that is 1-WL-Discriminating. After that, we will prove a composition lemma with Lemma 25 which is similar to the one we introduced in the previous section. From this point on, the proof continues as in the previous section and concludes the property to be proved in Lemma 26.

Lemma 23. Let G be an arbitrary graph with $n \coloneqq |V(G)|$ the number of nodes and $C : V(G) \to \mathbb{N}$ an arbitrary coloring of the graph G. Then the total number of possible tuples of the form:

$$(C(v),\ \{\!\{C(u) \mid u \in \mathcal{N}(v)\}\!\}),$$

for all $v \in V(G)$ can be upper bounded by:

$$n \cdot \sum_{i=0}^{n-1} \binom{n+i-1}{i}.$$

Proof. Assume the above. For the first entry of the tuple, at most n different colors exist since there are n nodes. For the second entry, each node $v \in V(G)$ can have between 0 and $n-1$ neighbors, such that the total number of possibilities is the sum over each cardinality of a multiset with n different colors. In the end, we soundly combine both results by multiplying both together. □

Lemma 24 (GNN 1-WL-Discriminating)**.** There exists a collection $\mathcal{C}$ of functions from $\mathcal{X}$ to $\mathbb{R}$ computable by GNNs that is 1-WL-Discriminating. Meaning for every $G_1, G_2 \in \mathcal{X}$ with $G_1 \not\simeq_{1\text{WL}} G_2$ there exists $\mathcal{A} \in C$ such that $\mathcal{A}(G_1) \neq \mathcal{A}(G_2)$.

Proof. Since $\mathcal{X}$ is finite, we define $n \coloneqq \max\{|V(G)| \mid G \in \mathcal{X}\}$ to be the maximum number of nodes of a graph in $\mathcal{X}$, and $k \coloneqq \max\{l_G(v) \mid v \in V(G), G \in \mathcal{X}\}$ to be the largest label of any node of a graph in $\mathcal{X}$. Using Lemma 23, we can compute an upper bound m using n for the number of distinct tuples. Note that, this bound holds true for all graphs in $\mathcal{X}$. We will now construct a GNN with n layers working on input G as follows:

$$f^{(0)}(v) \coloneqq l_G(v), \text{ and}$$
$$f^{(t)}(v) \coloneqq \mathsf{RELABEL}_{m,t}(f^{(t-1)}(v), \ \{\!\{f^{(t-1)}(u) \mid u \in \mathcal{N}(v)\}\!\}), \quad 0 < t < n.$$

Here $\mathsf{RELABEL}_{m,t}$ is a function, parametrized by m and t, that maps the tuples injectively to an integer of the set:

$$\{i \in \mathbb{N} \mid k + (t-1) \cdot m + 1 \leq i \leq k + t \cdot m\}.$$

This function exists as by the soundness of the upper bound of Lemma 23, the cardinality of its co-domain is greater or equal than the one of its domain. Thereby, and with the injectiveness of $\mathsf{RELABEL}_{m,t}$, we ensure that each GNN layer maps a tuple to a new, previously unused color. Therefore, every layer of this GNN computes a single iteration of the 1-WL algorithm. Further, since the 1-WL algorithm converges after at most $|V(G)| \leq n$ iterations, we set the number of layers to n, such that we ensure that the coloring computed by this GNN after n layers when applied on any graph $G \in \mathcal{X}$ is similarly expressive as the coloring computed by the 1-WL algorithm when applied on G.

We define the collection C of functions computable by GNNs that is 1-WL-Discriminating as:

$$C \coloneqq \{\mathcal{A} : \mathcal{X} \to \mathbb{R}, \ G \mapsto \mathsf{Readout}_c(\{\!\{f^{(n)}(v) \mid v \in V(G)\}\!\}) \mid c \in \mathbb{N}\},$$

where $\mathsf{Readout}_c$ is the Readout function that returns the number of nodes colored as c in the coloring of $f^{(n)}$. □

Similar to the proof in the previous section, we will use Lemma 25 to introduce the ability to construct GNNs that take in as input multiple GNNs and then apply a multilayer perceptron to the combined output.

Lemma 25 (GNN Composition)**.** Let C be a collection of functions computable by GNNs. Further, let $\mathcal{A}_1, \ldots, \mathcal{A}_n \in C$ and $\mathsf{MLP}^\bullet$ a suitable multilayer perceptron, then the function $\hat{\mathcal{A}}(\cdot) \coloneqq \mathsf{MLP}(\mathcal{A}_1(\cdot), \ldots, \mathcal{A}_n(\cdot))$ is also computable by a GNN.

Proof. Before we begin the proof, we briefly introduce two notations. For any $x \in \mathbb{R}^d$, we will use the notation $x[i]$ to indicate the i.th element of the vector x. Additionally, we indicate the merge and aggregation function used in layer t by $\mathcal{A}_i$ as $f^{(t)}_{\text{merge},i}$ and $f^{(t)}_{\text{agg},i}$. Similarly, does $\mathsf{Readout}_i$ indicate the Readout function and $f^{(0)}_i$ the input function of $\mathcal{A}_i$.

We will prove the lemma by giving a construction of a GNN model computing $\hat{\mathcal{A}}$. For the ease of readability and to reduce the complexity of the subsequent construction, we assume that for all $\mathcal{A}_i$ its functions $f^{(t)}_{\text{merge},i}, f^{(t)}_{\text{agg},i}$ and $\mathsf{Readout}_i$ map into the one-dimensional space $\mathbb{R}$

for all layers t. With this assumption, we avoid the need for a formal notation of the number of dimensions each of these functions map to.

Let T be the maximum number of layers of all $\mathcal{A}_1, \ldots, \mathcal{A}_n$. We construct the GNN $\hat{\mathcal{A}}$ with T layers, with the input layer working as follows on an input graph G:

$$\forall v \in V(G) : \ \hat{f}^{(0)}(v) \coloneqq \begin{bmatrix} f_1^{(0)}(v) \\ \vdots \\ f_n^{(0)}(v) \end{bmatrix},$$

and each other layer $0 < t \leq T$ utilizing the merge $\hat{f}^{(t)}_{\text{merge}}$ and aggregation $\hat{f}^{(t)}_{\text{agg}}$ functions as constructed in the following:

$$\hat{f}^{(t)}_{\text{merge}}(\hat{f}^{(t-1)}(v),\ Agg) := \begin{bmatrix} f^{(t)}_{\text{merge},1}(\hat{f}^{(t-1)}(v)[1],\ Agg[1]) \\ \vdots \\ f^{(t)}_{\text{merge},n}(\hat{f}^{(t-1)}(v)[n],\ Agg[n]) \end{bmatrix}, \quad \text{and}$$

$$\hat{f}^{(t)}_{\text{agg}}(\{\!\{\hat{f}^{(t-1)}(w) \mid w \in \mathcal{N}(v)\}\!\}) := \begin{bmatrix} f^{(t)}_{\text{agg},1}(\{\!\{\hat{f}^{(t-1)}(w)[1] \mid w \in \mathcal{N}(v)\}\!\}) \\ \vdots \\ f^{(t)}_{\text{agg},n}(\{\!\{\hat{f}^{(t-1)}(w)[n] \mid w \in \mathcal{N}(v)\}\!\}) \end{bmatrix}.$$

Note that, not all $\mathcal{A}_i$ will be comprised of T layers. For these cases we define the missing functions as follows:

$$f^{(t)}_{\text{merge},i}(\hat{f}^{(t-1)}(v),\ Agg) \coloneqq \hat{f}^{(t-1)}(v), \quad \text{and}$$
$$f^{(t)}_{\text{agg},i}(\{\!\{\hat{f}^{(t-1)}(w) \mid w \in \mathcal{N}(v)\}\!\}) \coloneqq 0.$$

These functions do not change anything and only forward the result of the actual computation of $\mathcal{A}_i$ to the last layer. Finally, we construct the $\mathsf{Readout}$ function of $\hat{\mathcal{A}}$ as follows:

$$\mathsf{Readout}(\{\!\{\hat{f}^{(T)}(v) \mid v \in V(G)\}\!\}) \coloneqq \mathsf{MLP}^{\bullet} \circ \begin{bmatrix} \mathsf{Readout}_1(\{\!\{\hat{f}^{(T)}(v)[1] \mid v \in V(G)\}\!\}) \\ \vdots \\ \mathsf{Readout}_n(\{\!\{\hat{f}^{(T)}(v)[n] \mid v \in V(G)\}\!\}) \end{bmatrix}.$$

With this, the proof concludes. Note that this proof can easily be extended to work without the assumption of each function mapping into a one-dimensional space. □

As a consequence of the previous two lemmas, we find ourselves in a similar position as at the beginning of the proof in Section 4.1. Specifically, we have established, through Lemma 24, the existence of a collection C of functions that can be computed by GNNs and can effectively distinguish any pair of graphs that are also distinguishable by the 1-WL algorithm. Furthermore, with Lemma 25, we have demonstrated that the composition of multiple GNNs and a multilayer perceptron remains computable by a single GNN. Consequently, we can also apply the findings of Lemmas 20 and 21 to GNNs. Thus, we can conclude that for any fixed $G^* \in \mathcal{X}$, the indicator function φ_{G^*} working over $\mathcal{X}$ with:

$$\forall G \in \mathcal{X} : \quad \varphi_{G^*}(G) := \begin{cases} 1, & \text{if } G \simeq_{1\text{WL}} G^* \\ 0, & \text{else} \end{cases},$$

is computable by a GNN.

Lemma 26. Let $\mathcal{C}$ be a collection of functions from $\mathcal{X}$ to $\mathbb{R}$ computable by GNNs so that for all $G^* \in \mathcal{X}$, there exists $\varphi_{G^*} \in \mathcal{C}$ satisfying $\forall G \in \mathcal{X} : \varphi_{G^*}(G) = \mathbb{1}_{G \simeq_{1\text{WL}} G^*}$. Then every function computable by 1-WL+NN is also computable by a GNN.

Proof. Assume the above. For any function $\mathcal{B}$ computed by 1-WL+NN that works over $\mathcal{X}$ to $\mathbb{R}$, we show that it can be decomposed as follows for any $G \in \mathcal{X}$ as input:

$$\begin{aligned}
\mathcal{B}(G) &= \Big(\frac{1}{|\mathcal{X}/\!\simeq_{1\text{WL}}(G)|} \sum_{G^* \in \mathcal{X}} \mathbb{1}_{G \simeq_{1\text{WL}} G^*} \Big) \cdot \mathcal{B}(G) \\
&= \frac{1}{|\mathcal{X}/\!\simeq_{1\text{WL}}(G)|} \sum_{G^* \in \mathcal{X}} \mathcal{B}(G^*) \cdot \mathbb{1}_{G \simeq_{1\text{WL}} G^*} \\
&= \sum_{G^* \in \mathcal{X}} \frac{\mathcal{B}(G^*)}{|\mathcal{X}/\!\simeq_{1\text{WL}}(G^*)|} \cdot \varphi_{G^*}(G) \qquad (0.5)
\end{aligned}$$

where we denote with $\mathcal{X}/\!\simeq_{1\text{WL}}(G^*)$ the set of all graphs G over $\mathcal{X}$ that are equivalent to G^* according to the $\simeq_{1\text{WL}}$ relation. Further, with Lemma 17 we know that for any $G_1, G_2 \in \mathcal{X}$ with $G_1 \simeq_{1\text{WL}} G_2 : \mathcal{B}(G_1) = \mathcal{B}(G_2)$.

We can encode $\mathcal{B}$ as stated in Equation 0.5 via a multilayer perceptron with $\frac{\mathcal{B}(G^*)}{|\mathcal{X}/\!\simeq_{1\text{WL}}(G^*)|}$ being constants and $\varphi_{G^*} \in \mathcal{C}$ encoding the indicator function. Combined with the Lemma 25, we can conclude that $\mathcal{B}$ is computable by a GNN. Important to note, we can only do this since $\mathcal{X}$ is finite, making the overall sum finite and the cardinality of $\mathcal{X}/\!\simeq_{1\text{WL}}(G^*)$ well-defined for all graphs. □

Part II.

Empirical Testing

The empirical part is divided into blbnalanb

5. Testing Configuration

This section delves into the configuration and setup of our empirical testing. We begin by presenting our carefully selected datasets, which serve as the foundation for our evaluation. We highlight specific insights and characteristics of these datasets that make them compelling choices for our study. Afterward, we focus on the models we employ for testing and subsequent result comparison. We provide a comprehensive overview of the selected models, outlining their key features and motivations behind their inclusion in our evaluation. Subsequently, we provide a detailed description of the training pipeline and explain specific hyperparameters for which we will optimize these models.

5.1. Datasets

We will first explain our choice of datasets and introduce each dataset individually. Afterward, we will explore essential observations that are to be considered when assessing the actual empirical results.

Choice of Datasets

In selecting the datasets for our thesis, we adhered to two fundamental principles to ensure the robustness and diversity of our evaluation for GNN and 1-WL+NN models. The first principle focuses on using widely recognized benchmark datasets that have been extensively employed in previous studies. This principle enables us and readers to make meaningful comparisons with existing results. The second principle focuses on choosing datasets that are distinct from one another in terms of both their application domains and the way they encode information in graphs.

To fulfill the first principle, we opted for datasets from the TUDataset library. This library, curated by Morris et al. [2020], serves as a widely recognized standard for evaluating graph-related methods.

Regarding the second principle, we incorporated the insights from Liu et al. [2022], who developed a comprehensive taxonomy of common graph benchmark datasets. Their work examined the degree to which information is encoded in graph structures compared to node features with respect to solving the task of the datasets. Based on their taxonomy, they categorized datasets into three distinct classes:

1. Datasets in which the most crucial information for solving the task is contained in the node features.
2. Datasets similar to the first category, but with the significant exception that the node degree strongly correlates with the node features. In these datasets, utilizing simple structural information, such as computing the node degree, is as beneficial for solving the task as using the original node features.
3. Datasets where the most crucial information is encoded within the graph structure itself.

These categories help us understand how information is encoded in various datasets, such that we aim to choose datasets from all three categories.

As a result of considering these two principles, we selected the following datasets for our thesis: Enzymes, Imdb-Binary, Mutag, Nci1, Proteins, and Reddit-Binary for classification tasks, and Alchemy and Zinc for regression tasks. For an overview of the elemental properties of each dataset, see Table 2. We will now shortly introduce each dataset individually:

Enzymes, provided by Borgwardt et al. [2005], is a dataset consisting of proteins in their tertiary structure, categorized into six distinct enzyme classes. Each node represents a secondary structure, and has an edge to its three spatially closest nodes. Furthermore, each node feature encodes the type of secondary structure (*helix*, *sheet* or *turn*), as well as physical and chemical information.

Imdb-Binary, provided by Yanardag and Vishwanathan [2015], is a dataset comprising ego networks. Each node in the network represents an actor/actress, and a unidirectional edge exists between two nodes if and only if the corresponding actors played together in a movie. The task involves determining whether each ego network's genre is *action* or *romance*.

Mutag, provided by Debnath et al. [1991], is a dataset comprising Nitroaromatic compounds. Each compound is represented by a graph in which nodes represent atoms, with their types encoded as node features, and edges represent atomic bonds. The task involves determining whether a given compound has a mutagenic effect on Salmonella typhimurium bacteria.

Nci1, provided by Wale et al. [2008], comprises graph representations of chemical compounds. In these graphs, nodes represent atoms, and edges represent atomic bonds. Moreover, the atom types are encoded in the node features. The overall task involves determining whether a given compound is active or inactive in inhibiting non-small cell lung cancer.

Proteins, provided by Borgwardt et al. [2005], contains proteins encoded similarly to ENZYMES. The task here is to determine whether each graph represents an enzyme.

Reddit-Binary, provided by Yanardag and Vishwanathan [2015], involves graphs that are derived from popular Reddit communities. The nodes in these graphs represent users who are active in the community, while the edges represent interactions between the users. The task is to identify whether a graph belongs to a community that is focused on questions and answers, or one that is focused on discussions.

Alchemy, provided by Chen et al. [2019], consists of organic molecules, with each node representing an atom and each edge representing an atomic bond. Additionally, each node feature encodes various properties for each atom, while each edge encodes the bond type and distance between atoms. The overall task is to compute 12 different continuous quantum mechanical properties for each graph.

Zinc, provided by Bresson and Laurent [2019] and Irwin et al. [2012], consists of molecular graphs where each node represents a heavy atom, and the corresponding node feature specifies its type. The edges in the graph encode the bonds between atoms, and their features further describe the type of bond. The task is to calculate a molecular property known as constrained solubility ($\log P - \mathrm{SA} - \mathrm{cycle}$).

Table 2.: Dataset statistics and properties for graph-level prediction tasks. This table has been adapted from Morris et al. [2022].

	Dataset	Properties						
		Number of graphs	Number of classes/targets	∅ Number of nodes	∅ Number of edges	Node labels	Edge labels	Taxonomy Category
Classification	Enzymes	600	6	32.6	62.1	✓	✗	1
	IMDB-Binary	1 000	2	19.8	96.5	✗	✗	3
	Mutag	188	2	17.9	19.8	✓	✗	2
	NCI1	4 110	2	29.9	32.3	✓	✗	3
	Proteins	1 113	2	39.1	72.8	✓	✗	2
	Reddit-Binary	2 000	2	429.6	497.8	✗	✗	3
Reg.	Alchemy	202 579	12	10.1	10.4	✓	✓	-
	Zinc	249 456	1	23.1	24.9	✓	✓	-

Analysis of the Datasets

To ensure the reliability and fairness of our evaluation, one of our initial steps was to assess the balance of our selected datasets for classification. We employed the normalized Shannon index to evaluate the balance of a dataset, where a value close to 0 indicates maximum imbalance, while a value close to 1 signifies perfect balance. See Appendix 1.1 in the Appendix for a formal definition of this metric.

Table 3.: An overview of the normalized Shannon index calculated for each dataset.

	Dataset					
	Enzymes	Imdb-Multi	Mutag	NCI1	Proteins	Reddit-Binary
Shannon index	1	1	0.920	1	0.973	1

Table 3 provides an overview of the normalized Shannon index computed for each selected classification dataset. Upon analyzing the data, we observed that all the datasets exhibit high balance, as all their values are close to 1. This finding assures us that the datasets do not suffer significant class imbalances, which will remain important in the following section.

In addition to the balance of all datasets, another important aspect is understanding the upper bound of performance achievable by both GNN and 1-WL+NN models on these datasets. Unlike in other areas of machine learning where multilayer perceptron models can achieve near-perfect performance due to their universal approximation capabilities (Hornik [1991]), GNN and 1-WL+NN models have inherent limitations on their expressiveness. This restriction stems from the fact that the expressiveness of the 1-WL algorithm limits the performance of both frameworks. In detail, if the 1-WL algorithm can not distinguish a pair of graphs in a dataset, then neither a GNN nor a 1-WL+NN model can.

While we have pointed out that the 1-WL algorithm is, in general, quite powerful in distinguishing pairs of graphs in Section 2; we also explained that it is not complete. Therefore, assuming that GNN or 1-WL+NN models exist that can achieve almost perfect accuracy on all classification datasets is not reasonable. Thus, we calculated the theoretical maximum accuracy achievable by the perfect model for each dataset. In detail, we even investigated how

many iterations of the 1-WL algorithm it takes to achieve this accuracy. For a comprehensive overview of the accuracies achievable on all datasets, please refer to Table 4. In this table, we have included the accuracy achievable when running the 1-WL algorithm for 0 iterations, which essentially means taking the initial node features as the coloring for iteration 0 and assessing the expressiveness of this initial coloring.

Table 4.: An overview of the maximum theoretical classification accuracy achievable for each dataset based on the number of 1-WL iterations in percent. A hyphen "-" indicates that the maximum accuracy has converged with fewer iterations, implying that further iterations do not improve the accuracy.

1-WL	**Dataset**					
	ENZYMES	IMDB-BINARY	MUTAG	NCI1	PROTEINS	REDDIT-BINARY
Iterations: 0	81.4	60.6	93.1	91.3	91.9	83.9
Iterations: 1	100.0	88.6	95.7	99.5	99.7	100.0
Iterations: 2	-	-	99.5	99.8	-	-
Iterations: 3	-	-	100.0	99.8	-	-
Iterations: 4	-	-	-	-	-	-
Max Accuracy	100.0	88.6	100.0	99.8	99.7	100.0

Upon examining the results, we observe that all datasets exhibit perfect or near-perfect theoretical classification accuracies. This result makes interpreting results obtained from actual 1-WL+NN or GNN models later on more straightforward. Additionally, the accuracy achievable after each number of iterations provides a theoretical lower limit on the number of message-passing layers a GNN must be composed of to be even capable of achieving this accuracy.

We have conducted the same analyzes on additional datasets, as their results might be valuable to the reader. For these, see Table B.1 in the Appendix.

5.2. Choice of Models

In selecting our models, we aimed to use techniques that are relatively generic and not highly specialized for any of the datasets, such that insights we gain upon analyzing the model's performance can be generalized better. Consequently, we opted for a basic set of models to maintain simplicity and versatility.

1-WL+NN Models

Our primary consideration for the 1-WL+NN models revolves around choosing an encoding function, as all other components are fixed. To keep things straightforward, we decided to employ encoding functions consisting of two main components. Firstly, an optional preprocessing step that operates on the colors computed by the 1-WL algorithm. Secondly, a basic pooling function for transforming the color histogram into a fixed-size vector.

In more detail, the optional preprocessing step involves a simple look-up table. If utilized, this step maps each color injectively to a vector in the range of $[-1, 1]^n$, where the value of n is a hyperparameter. By encoding the color information into higher dimensions, this approach aims to enhance efficiency during subsequent processing steps. For the second step, the pooling

component, we selected elementary functions such as elementwise Max, Mean, and Summation (Sum). In summary, each of the 1-WL+NN models can be uniquely identified by their encoding functions; therefore, we will refer to each model by their encoding function as follows:

$$\text{Embedding} - \{\mathsf{Max}, \mathsf{Mean}, \mathsf{Sum}\} \quad \text{or} \quad \{\mathsf{Max}, \mathsf{Mean}, \mathsf{Sum}\},$$

where "Embedding" indicates the use of the optional preprocessing step.

GNN Models

As mentioned in the introduction to this section, our focus is on keeping the models basic. Hence, we opted for GIN by Xu et al. [2019], GCN by Kipf and Welling [2017], and GAT by Veličković et al. [2017] as the base architecture for the message-passing layers. Each of these architectures was chosen for specific reasons.

Firstly, we included GIN as an obvious candidate because it has been proven to be as expressive as the 1-WL algorithm. This characteristic makes it interesting when comparing it to 1-WL+NN models. Next, we also included GCN based on its good empirical success in recent years. Furthermore, the insights provided by Nikolentzos et al. [2023a] demonstrated that, in a certain sense, the node features computed by GCN and GIN are similar, making GCN a reasonable alternative to GIN in cases where the advantage of GIN's expressiveness is not needed. Lastly, we added GAT as an alternative approach to the other two architectures. In detail, Nikolentzos et al. [2023a] also showed that the node features computed by GAT are entirely different from those computed by GIN or GCN.

Regarding the choice of Readout functions, we decided to utilize functions that are composed of two components. The first component is one of the elementwise pooling functions, such as Max, Mean, and Sum, to aggregate the information from a graph representation into a fixed-sized vector. Secondly, we incorporate a multilayer perceptron to process the aggregated information further, similarly to the 1-WL+NN models.

In summary, each of the GNN models can be uniquely identified by their GNN architecture and the pooling function utilized; therefore, we will refer to each model by these two properties as follows:

$$\{\mathsf{GAT}, \mathsf{GCN}, \mathsf{GIN}\} - \{\mathsf{Max}, \mathsf{Mean}, \mathsf{Sum}\}.$$

Note that the selection of the Readout function creates similarities between the GNN and 1-WL+NN models. These similarities play a crucial role in ensuring that any empirical differences observed between the two frameworks are not attributed to the utilization of more powerful techniques.

5.3. Experimental Setup

For the empirical testing, we took measures to ensure the reliability of our results in terms of hyperparameter configuration. Additionally, we aimed to ensure the reproducibility of the training pipeline for each model.

Testing Procedure

We started by conducting tests on the classification datasets, which serve as the basis for our evaluation. In our testing code, we employ a 10-fold cross-validation approach. Within this framework, we further partitioned the training data randomly, allocating 10 % of it for

validation purposes. Consequently, each training iteration consisted of 81 % of the original dataset as the training set, 9 % as the validation set, and 10 % as the test set. We repeat this testing procedure five times to mitigate the influence of randomness on the model's performance. Ultimately, we recorded the mean accuracy on the test set along with its standard deviation as the primary performance metric of the model. Note that the use of standard cross-validation for generating the splits and the choice of mean accuracy as our primary metric is reasonable and justified as the datasets are highly balanced, as demonstrated in Section 2.

In the case of the regression datasets, we adopted a slightly different testing procedure. Due to their larger scale compared to the classification datasets, we opted for a more time-efficient approach. To achieve this, we utilized pre-existing training pipelines developed in Morris et al. [2020] and Morris et al. [2022]. These pipelines use a fixed training, validation, and test split, accelerating the testing process. Similar to the classification datasets, we performed five runs for each model configuration and conducted a hyperparameter sweep for all model configurations. We record the mean absolute error and its standard deviation, as well as the mean logarithmic absolute error and its standard deviation across all runs. Furthermore, we test two splits for each regression dataset: one utilizing only 10 000 samples for training, while the other split uses the entire training set.

Say that due to these reasons our main focus in testing is on the classification datasets!

Hyperparameter Optimization

To ensure the comparability of our results with other works and limit the number of hyperparameters requiring optimization, we followed standard practices when configuring our models. Detailed information on all hyperparameters, including the ones we optimized, can be found in Table B.2 for the 1-WL+NN models used in classification tasks, Table B.3 for the GNN models employed in classification tasks, and Table B.4 for the 1-WL+NN models utilized in the regression task in the Appendix. We will shortly discuss the most critical parameters we optimized for:

Early in our investigations, we made a significant observation regarding the learning performance of 1-WL+NN models. We noticed considerable performance discrepancies when comparing 1-WL+NN models using the standard version of the 1-WL algorithm with the one from GNN's. Consequently, we investigated the possibility of parametrizing the 1-WL algorithm to enhance control over the expressiveness of the colorings it computes. Specifically, we focused on two crucial parameters: 1) the number of iterations and 2) the usage of its convergence behavior as an early termination criterion.

The advantage of this more granular parametrization is that it enables us to apply the same number of 1-WL iterations to each graph processed by a 1-WL+NN model by deactivating the convergence behavior and fixing the number of iterations. By deactivating this behavior and keeping the number of iterations minimal, we observed that the number of colors used by the 1-WL algorithm remained contained. As a result, the MLP component of each 1-WL+NN model seems to generalize better, significantly improving performance. Therefore, one of the most crucial hyperparameters we optimized for all 1-WL+NN models was the number of 1-WL iterations. Additionally, if employed, the size of the dimension of the look-up table was another significant parameter to optimize.

In contrast, the hyperparameter selection for the GNN models was relatively less intricate. The key parameters of interest here are the number of message-passing layers and the size of the hidden dimensions used in each layer. The reason for this is that the number of layers directly corresponds to the expressiveness of the GNN, as demonstrated in the proof, while the size of the hidden dimensions enables easier learning by allowing the model to store more

information during graph processing.

Implementation Details and Result Accessibility

The implementation of our models and training procedures was carried out using Python 3.10 along with the open-source library PyTorch[6] and its extension PyTorch Geometric[7]. Moreover, we leveraged Weights&Biases as our tool for coordinating and recording the results of the hyperparameter optimization. The code for our experiments is publicly available on GitHub at `https://github.com/ericbill21/BachelorThesis`, and the corresponding results can be accessed via Weights&Biases at `https://wandb.ai/eric-bill/BachelorThesisExperiments`. We conducted our tests on the RWTH High Performance Computing cluster by the RWTH Aachen University as well as on private hardware.

6. Empirical Testing

In this section, we present the empirical findings of our study. A total of 5 581 runs were conducted, with each run testing a specific model configuration on a designated dataset. These runs required a substantial amount of computation time, totaling 1 644 hours (over 70 days). To examine the classification accuracy achieved by the best-performing configuration of each model on each classification dataset, please refer to Table 5. For regression datasets, Table 6 provides an overview of the mean absolute error (MAE) for the best-performing configurations.

Due to the significantly larger size of the regression datasets compared to the classification datasets, running regression experiments required considerable time for each configuration. As a result, we had to limit the number of different configurations tested. For this reason, we employed existing training pipelines, as mentioned in the previous section, which allowed us to include the results of the GINE-ε model proposed by Morris et al. [2020] and Morris et al. [2022] in Table 6. The GINE-ε model utilizes the GIN architecture for message-passing layers, Mean as its pooling function, and a two-layer MLP for the final processing of its input graph. This design closely resembles our GIN:Mean model, with the crucial distinction being that GINE-ε incorporates edge features in its computations.

The decision to exclude edge features from all our models, including all 1-WL+NN models, was driven by two key factors. Firstly, our focus primarily revolved around the classification datasets, all of which do not encode any information in their edge features (refer to Table 2). Secondly, the regression datasets we utilized in our evaluation include continuous edge features, making the application of the 1-WL algorithm more complex. Although some work exists on modifying the 1-WL algorithm to incorporate continuous features, we opted for a more straightforward and more scalable approach by not considering edge features in the computations of all our models. Nonetheless, this limitation does not compromise the integrity of our results, as our main objective is to compare similar GNN and 1-WL+NN models. The inclusion of GINE-ε showcases the potential and highlights the significance of edge feature information for solving the dataset tasks of Alchemy and Zinc.

A notable finding when analyzing the presented results is that the performance of 1-WL+NN models is comparable to that of GNN models. In fact, the best 1-WL+NN models even

[6] A free and open-source machine learning framework that was originally developed by Meta AI and is now part of the Linux Foundation umbrella. https://pytorch.org

[7] An open-source library that extends PyTorch and allows for easy development and training of graph neural networks. https://pytorch-geometric.readthedocs.io

outperform the GNN models in all classification datasets, with the exception of IMDB-BINARY and REDDIT-BINARY. These two datasets stand out among the classification datasets as they lack node features. We will investigate this insight later on in more detail. Moreover, our results align with the empirical findings of other GNN models in various studies. The accuracy reported here falls within a similar range as observed in works by Xu et al. [2019], Morris et al. [2022, 2020], Zhang et al. [2018].

In the subsequent subsection, we will further analyze these results. Specifically, we will investigate the tradeoff between generality and expressiveness in 1-WL+NN models, the learned aggregation functions of each model, the ability of GNN models to approximate 1-WL+NN models, the differences in their learning behaviors, and the impact of GNN models performance by preprocessing the data.

Table 5.: Overview of the mean classification accuracies achieved by the best configuration of each model for each dataset in percent and standard deviation.

	Method	Dataset					
		ENZYMES	IMDB-BINARY	MUTAG	NCI1	PROTEINS	REDDIT-BINARY
1-WL+NN	Max	16.7 ±4.2	52.0 ±5.3	73.8 ±12.4	58.6 ±3.3	62.9 ±4.9	69.2 ±4.0
	Mean	18.2 ±4.8	59.4 ±5.8	77.1 ±11.5	64.0 ±3.3	60.9 ±4.5	66.1 ±3.2
	Sum	18.0 ±6.2	57.5 ±5.1	66.8 ±13.9	56.9 ±3.8	65.6 ±4.8	73.0 ±5.1
	Embedding-Max	40.5 ±7.4	69.4 ±4.9	81.1 ±11.2	82.7 ±2.0	**75.2** ±3.9	71.1 ±3.9
	Embedding-Mean	42.6 ±9.0	**72.4** ±4.1	84.1 ±9.1	83.1 ±1.9	72.3 ±4.2	75.4 ±2.8
	Embedding-Sum	**48.3** ±8.1	72.0 ±3.8	**85.1** ±8.6	**83.6** ±2.2	75.2 ±4.5	**78.4** ±2.7
Graph Neural Networks	GAT:Max	31.2 ±6.0	70.7 ±4.8	71.1 ±12.2	58.0 ±4.2	72.5 ±5.1	77.7 ±5.0
	GAT:Mean	28.9 ±5.9	70.9 ±3.7	74.8 ±9.1	66.1 ±2.8	64.9 ±6.4	70.0 ±6.9
	GAT:Sum	**34.4** ±7.0	72.2 ±4.5	82.1 ±11.2	69.8 ±2.6	73.4 ±3.9	78.1 ±4.2
	GCN:Max	33.1 ±7.5	73.5 ±4.1	74.5 ±11.3	61.1 ±3.6	69.8 ±5.9	74.3 ±4.5
	GCN:Mean	29.9 ±5.7	**74.7** ±3.8	75.0 ±10.4	68.9 ±2.4	70.9 ±5.2	82.3 ±3.3
	GCN:Sum	31.7 ±7.2	73.0 ±4.4	81.5 ±10.3	70.4 ±2.1	3.5 ±3.9	**86.9** ±3.2
	GIN:Max	29.2 ±6.2	70.8 ±4.7	77.3 ±10.7	**79.9** ±2.2	**74.3** ±5.1	76.1 ±3.6
	GIN:Mean	31.7 ±6.7	71.1 ±5.4	82.4 ±9.8	70.8 ±2.2	72.0 ±4.0	73.5 ±3.8
	GIN:Sum	28.9 ±8.7	69.5 ±4.8	**84.6** ±8.7	70.8 ±2.3	74.0 ±4.3	74.0 ±4.3

6.1. Fixed 1-WL Iterations: Tradeoff between Expressiveness and Generality

As discussed in Section 5.3, we explored constraining the expressiveness of the 1-WL algorithm by fixing the number of iterations it is applied to each graph in a 1-WL+NN model. The intention behind this was to ensure that the resulting colorings of graphs computed using a fixed 1-WL algorithm would fall within a similar color range, thereby limiting the total number of colors and avoiding outlier cases.

From a theoretical perspective, fixing the number of 1-WL iterations in a 1-WL+NN model only limits its expressiveness. For the remainder of this section, we will denote the number of 1-WL iterations by $n_{\mathsf{wl}} \in \mathbb{N}$. For instance, let $n_{\mathsf{wl}} \in \mathbb{N}$ now be fixed. If the standard 1-WL algorithm converges on an input graph G after $k' < k$ iterations, the coloring computed after n_{wl} iterations is as expressive as the one obtained from the standard 1-WL algorithm since the coloring convergence after k' iterations. On the contrary, if the standard 1-WL algorithm

Table 6.: Overview of the mean absolute error and the standard deviation (logMAE) on large-scale (multi-target) molecular regression tasks. The results marked by [1] are adopted from Morris et al. [2020] and by [2] from Morris et al. [2022].

	Method	Dataset			
		Alchemy	Alchemy (10k)	Zinc	Zinc (10k)
	GINE-ε[1,2]	0.103 ±0.001 -2.956 ±0.029[1]	0.180 ±0.006 -1.958 ±0.047[2]	-	0.084 ±0.004[1]
GNN	GIN:Max	0.604 ±0.004 -0.578 ±0.009	0.353 ±0.003 -1.228 ±0.006	0.124 ±0.004	0.427 ±0.009
GNN	GIN:Mean	0.643 ±0.014 -0.505 ±0.021	0.314 ±0.004 -1.469 ±0.044	0.110 ±0.005	0.341 ±0.037
GNN	GIN:Sum	**0.523** ±0.016 -0.705 ±0.035	**0.282** ±0.002 -1.890 ±0.031	**0.104** ±0.005	**0.298** ±0.034
1-WL+NN	Embedding-Max	0.648 ±0.003 -0.511 ±0.009	0.409 ±0.003 -1.023 ±0.009	0.382 ±0.005	0.659 ±0.007
1-WL+NN	Embedding-Mean	0.617 ±0.003 -0.564 ±0.005	0.355 ±0.004 -1.269 ±0.020	**0.348** ±0.010	0.484 ±0.009
1-WL+NN	Embedding-Sum	**0.600** ±0.004 -0.625 ±0.032	**0.305** ±0.001 -1.740 ±0.042	0.384 ±0.004	**0.465** ±0.009

converges after $k' > k$ iterations on an input graph G, the coloring obtained after n_{wl} iterations is less expressive and contains less information than the coloring derived from the standard 1-WL algorithm.

Comparing the performance of 1-WL+NN models utilizing the standard 1-WL algorithm to those using the parametrized version reveals a significant difference across all classification datasets, as seen in Table 7. This data confirms our belief that the standard 1-WL algorithm can be overly expressive for specific tasks, as evidenced by the considerable performance gap between the two types of the algorithm. Additionally, we included the mean number of iterations of the 1-WL algorithm applied on each dataset graph in the brackets in Table 4. This number remains a fixed constant for the models utilizing the parametrized version.

Algorithm Type	Dataset					
	Enzymes	Imdb-Binary	Mutag	NCI1	Proteins	Reddit-Binary
Standard 1-WL	34.2 ±6.7 ($\varnothing n_{\mathsf{wl}}$: 3.0)	67.0 ±4.3 ($\varnothing n_{\mathsf{wl}}$: 1.2)	76.3 ±9.4 ($\varnothing n_{\mathsf{wl}}$: 4.2)	78.9 ±2.1 ($\varnothing n_{\mathsf{wl}}$: 3.9)	71.4 ±4.9 ($\varnothing n_{\mathsf{wl}}$: 3.0)	70.9 ±3.8 ($\varnothing n_{\mathsf{wl}}$: 4.1)
Parametrized 1-WL	48.3 ±8.1 (n_{wl} : 1)	72.4 ±4.1 (n_{wl} : 1)	85.1 ±8.6 (n_{wl} : 1)	83.6 ±2.2 (n_{wl} : 3)	75.2 ±3.9 (n_{wl} : 1)	78.4 ±2.7 (n_{wl} : 1)

Table 7.: Comparison between the best performing 1-WL+NN models using the standard 1-WL algorithm and the one employing the parametrized version of it in percent and standard deviation. Additionally, we put the average number of iterations of the 1-WL algorithm in brackets for each model.

Building on these insights, investigating the optimal number of 1-WL iterations that lead to the best-performing models is another interesting observation. To illustrate its effect, we created Figure 7, which showcases the performance achieved by all models and configurations grouped by the number of 1-WL iterations for each dataset in a violin graph. Note that both classification and regression datasets are included in this figure. Depending on the dataset type, the y-axis represents either classification accuracy or test error, where higher accuracies imply better performance for classification tasks, and higher test errors imply poorer performance for regression tasks (and vice versa).

In general, the results indicate that the performance of 1-WL+NN models tends to improve as the number of 1-WL iterations decreases, except for NCI1, Alchemy and Zinc datasets.

Notably, for NCI1, the optimal number of iterations coincides with the number of 1-WL iterations needed for the maximum achievable accuracy (refer to Table 4). This correlation

holds for all other classification datasets, except for MUTAG. However, the behavior observed in MUTAG can potentially be attributed to the fact that according to the introduced taxonomy (Liu et al. [2022]) in Section 5.1, MUTAG can be effectively solved by simply replacing its node features with an encoding of the node degree. Since, from a theoretical perspective, the coloring computed after the first iteration of the 1-WL algorithm is usually an encoding of the node degree, this might explain the observed pattern.

Interpreting the results of the ZINC dataset is more complex and somewhat peculiar. While the smaller subset of the dataset, ZINC10K, clearly indicates that fewer 1-WL iterations yield better results, the overall ZINC dataset suggests the opposite. This discrepancy could be attributed to the limited number of runs conducted on the entire dataset, which were restricted due to scalability and time constraints. Therefore, these results should be interpreted with caution.

In conclusion, reducing the number of 1-WL iterations leads to improved generability and overall better performance of the models, with the clear exception of NCI1. However, as our results indicate, most 1-WL+NN models achieve optimal performance when employing only a single iteration of the 1-WL algorithm, which is essentially equivalent to encoding the node degree. This observation demonstrates that 1-WL+NN models do not require the full expressiveness of the 1-WL algorithm to achieve comparable performance to GNN models, which raises the question of whether GNN models, despite their theoretical ability to be highly expressive, also tend to rely primarily on node degree information for computation. We will explore this question further in Section TODO.

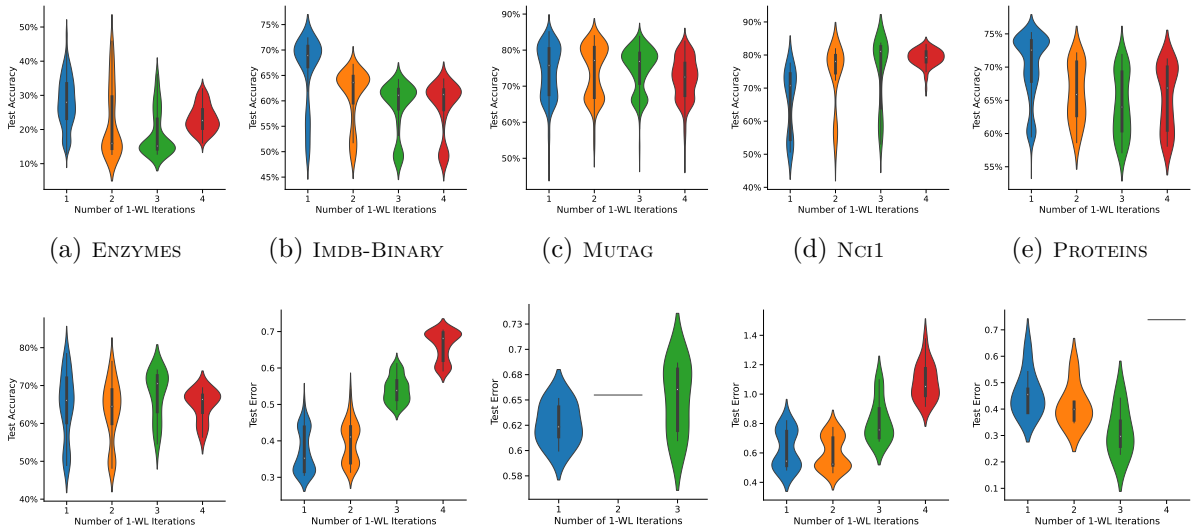

(a) ENZYMES (b) IMDB-BINARY (c) MUTAG (d) NCI1 (e) PROTEINS

(f) REDDIT-BINARY (g) ALCHEMY (10K) (h) ALCHEMY (i) ZINC (10K) (j) ZINC

Figure 7.: Impact on performance by the number of itertations of the 1-WL alogirhtm.

6.2. Difference in Learning behavior

The learning behavior of 1-WL+NN models presents a challenge due to the expressiveness of the 1-WL algorithm, which directly impacts their performance. One notable distinction between 1-WL+NN and GNN models is the significant discrepancy observed between their training and test performance. While it is typical to witness higher training performance compared to testing

performance in various machine learning applications, this difference is particularly pronounced in 1-WL+NN models. Figure 5 illustrates this discrepancy across all classification datasets. We considered different subsets from the best-performing models, ranging from the top 1 % to the top 100 %. Each bar represents the mean difference between the training accuracy and the test accuracy of the respective quantile of runs. The models trained with 1-WL+NN are depicted in blue, while those trained with GNN are represented in orange. The height of each bar indicates the degree of overfitting, with taller bars suggesting more substantial overfitting and poor generalization, while shorter or even negative bars indicate better generalization, where the performance on the training set aligns more closely with the performance on the testing set. The black line in each bar denotes the standard error.

Analyzing the figure reveals that 1-WL+NN models tend to exhibit more significant overfitting compared to GNN models, particularly in datasets such as Enzymes, Mutag, Proteins, and Reddit Binary. For instance, in the case of Enzymes, the top 1 % of best-performing 1-WL+NN models display, on average, a 27 % higher training accuracy than their test accuracy, highlighting the extent of overfitting with 1-WL+NN models.

While GNN models also experience some overfitting, mainly observed in the NCI1 dataset, it is not as prevalent across all datasets and not as dramatic as in the case of 1-WL+NN models. Moreover, in datasets like Mutag or Reddit Binary, it demonstrates the superior generalization capability of GNN models. In these cases, the difference in performance is close to 0 %, and in the case of Mutag, it is even negative. This indicates that GNN models were able to learn general patterns in these datasets rather than memorizing the data.

This raises the question of why 1-WL+NN models tend to exhibit such dramatic overfitting. We hypothesize that the 1-WL algorithm's excessive expressiveness leads to the computation of highly detailed colorings of the input graphs.

To gain insight into the algorithm's expressiveness, we calculated the ratio of unique colors compared to the total number of possible colors for each dataset. For example, the ENZYMES dataset consists of 600 graphs, with a total of 19,580 nodes. This number represents an upperbound on the number of different colors that can be present in the colorings computed by the 1-WL algorithm when applied to Enzymes. After a single iteration, all colorings consist of only 231 colors, accounting for less than 0.01 % of the total number of colors that could be used. However, after another iteration, resulting in a total of two iterations of the 1-WL algorithm, this number has already increased to 10,416, comprising 53.2 % of the total available colors. This clearly demonstrates the significant expressiveness of the colorings after just a few iterations.

Figure 9 illustrates this ratio of unique colors used compared to the total possible colors (total number of nodes in each dataset). As expected, the ratio converges with additional 1-WL iterations due to the convergence behavior of the algorithm. However, it is evident that the ratio rises rapidly and dramatically for all datasets. We included an enlarged section of the initial part of the plot to emphasize that even a small ratio around 10 % signifies a large number of unique colors in the colorings computed by the 1-WL algorithm. To contextualize each value, refer to Table 2 to estimate the total number of nodes in each dataset or consult Table 4 in the Appendix, which lists the number of unique values for each dataset.

Another point to emphasis is that the colors have nothing to do with antoher in a wl coloring have almost nothing to do with another. Meaning, for example if two nodes are colored by two distinct integers which are close thogher, this does not mean that both nodes are in anyway similar to another structurally. Allthoug, we use in our expermirements an implementation of the 1-WL alogrithm that assings each node alwasy the smallest unused colors, a connection

between colors is still not really existend due shuffeling the dataset when applying the 1-WL alogiorhtm.

After seeing how the number for colors for wl iteration greater equal to two almost explodes and we see this as the primary reason for the overfitting behavior it begs the question if this can also be seen in our data. For this reasons we plotted figure 11, which is the exact same graphic as used before, with the differnec that now, we do not compare both framewokrs, bit only consider 1-WL+NN models and compare the different number of 1-WL iterations. Accross all classification datasets, we see that the overfitting behvaior compared to using only a sinle iteration of the 1-WL algorithm is more substantial. Thebery configrming our believes. Also as expected in the majority of datasets we even see that with an increased 1-WL iterations the overftiiting behvaior gets worse. In the case of Enzymes, the train accuracy is on average over 60 % higher than the test accuracy. Demonstrating just, how worse it this overfitting behaviour gets with increased number of 1-WL iterations.

In conclusions this shows that 1-WL+NN models are only good in generalization when keeping the number of 1-WL iterations to 1. Otherwise this overfitting behvaior sets in. This insight shows that the expressivesness of 1-WL is too much, and that in comparisoon gnn are able to learn a very good and genral represetntion of tgheir graphs.

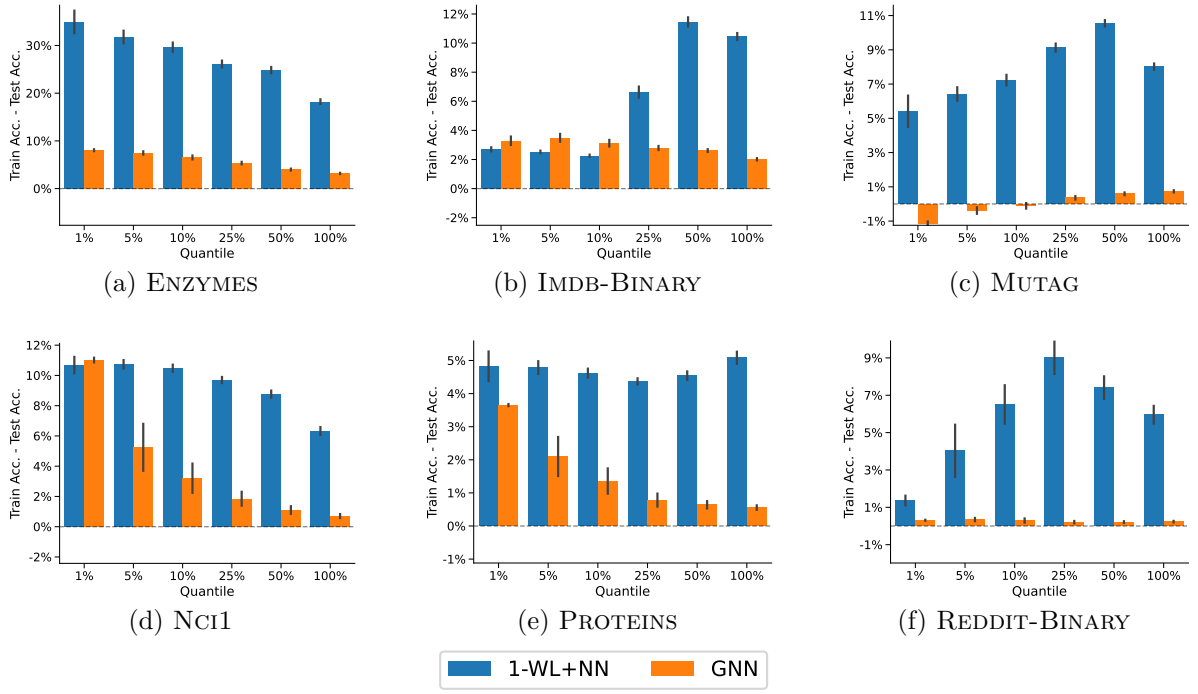

(a) Enzymes (b) Imdb-Binary (c) Mutag

(d) Nci1 (e) Proteins (f) Reddit-Binary

Figure 8.: Mean absolute difference of the classification accuracies of the training and testing set of each dataset. In detail, we compared the different quantiles of each performance.

6.3. Aggregation Differnces

6.4. GNN Approximating 1-WL

6.5. Preprocessing Data for GNNs

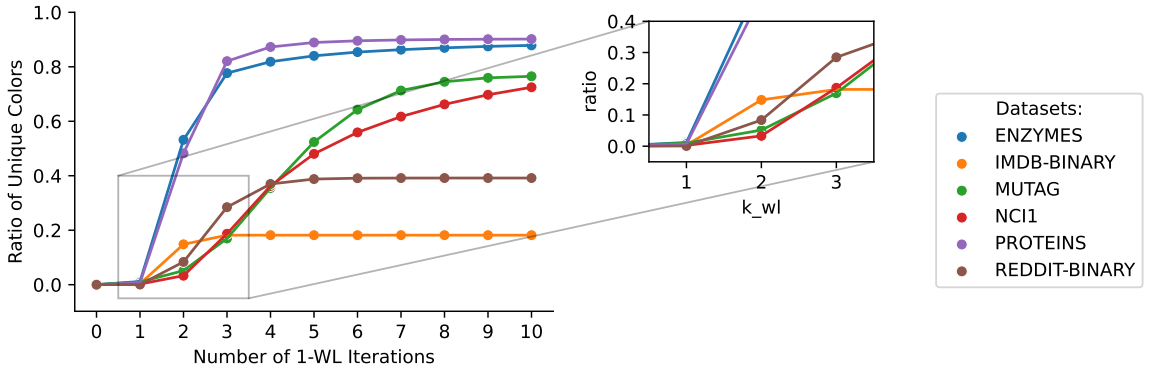

Figure 9.: Overview of the colors

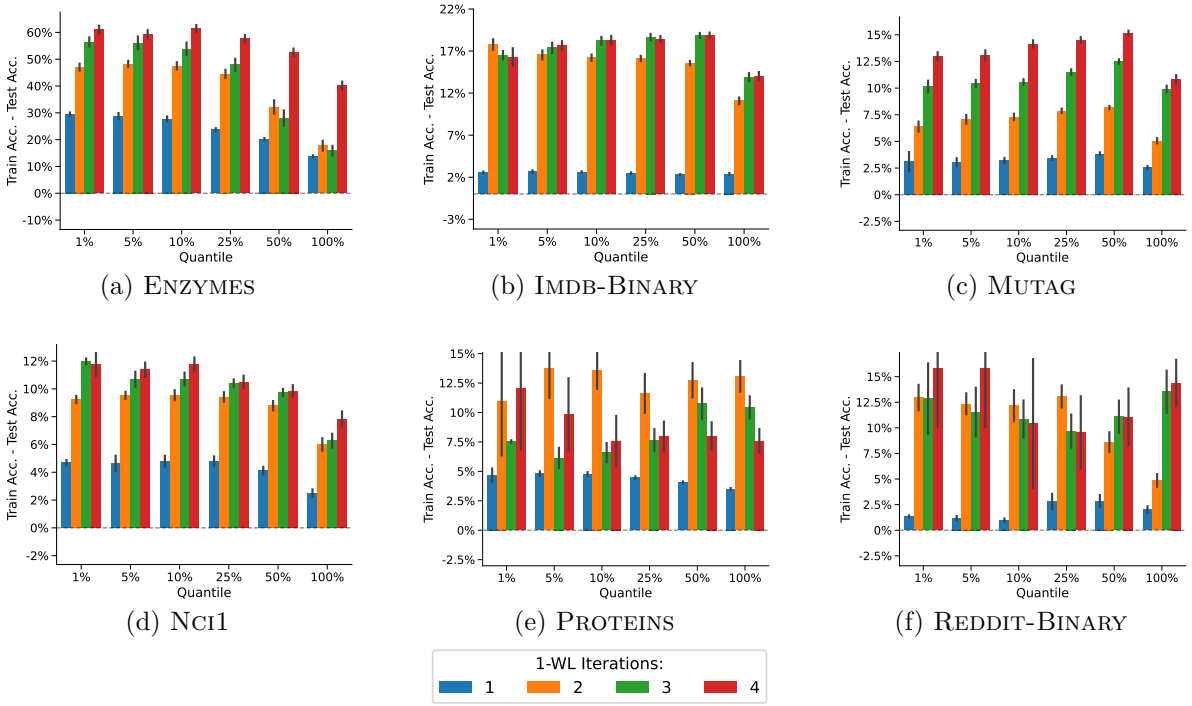

(a) Enzymes (b) Imdb-Binary (c) Mutag

(d) Nci1 (e) Proteins (f) Reddit-Binary

7. Discusssion

7.1. Learned Lessons

7.2. Future Work

8. Conclusion

	Method	Dataset					
		ENZYMES	IMDB-BINARY	MUTAG	NCI1	PROTEINS	REDDIT-BINARY
1-WL+NN	MLP	48.3 ±8.1	**72.4** ±4.1	85.1 ±8.6	83.6 ±4.1	**75.2** ±3.9	
	SVM Linear	34.4 ±5.5	71.2 ±3.9	86.4 ±8.9	83.4 ±2.1	73.9 ±4.1	
	SVM RBF	45.0 ±7.0	72.8 ±4.3	83.2 ±7.5	83.6 ±1.9	75.2 ±4.0	
	k-NN	**56.3** ±5.8 (k=1)	72.3 ±4.1 (k=11)	**86.7** ±7.7 (k=10)	**83.9** ±1.8 (k=5)	73.9 ±4.1 (k=19)	
GNN	MLP	34.4 ±7.0	**74.7** ±3.8	84.6 ±8.7	**79.9** ±2.2	74.3 ±5.1	
	SVM Linear	33.2 ±5.9	73.9 ±4.2	51.9 ±34.1	67.4 ±2.2	74.7 ±4.2	
	SVM RBF	35.9 ±6.0	74.1 ±3.9	**86.0** ±7.4	73.0 ±1.9	74.6 ±4.6	
	k-NN	**51.6** ±7.0 (k=1)	74.3 ±4.0 (k=132)	88.3 ±6.5 (k=38)	77.5 ±1.7 (k=2)	**74.9** ±4.3 (k=27)	

Table 8.: Overview of the classification accuracies achieved by the best model for each dataset in percent and standard deviation. Additionally, the performance of each model was evaluated under alternative configurations, namely the substitution of the Multilayer Perceptron (MLP) with a Support Vector Machine employing either a linear kernel (SVM Linear) or the Radial Basis Function (SVM RBF), as well as the k-nearest neighbors algorithm (k-NN) with different values for k.

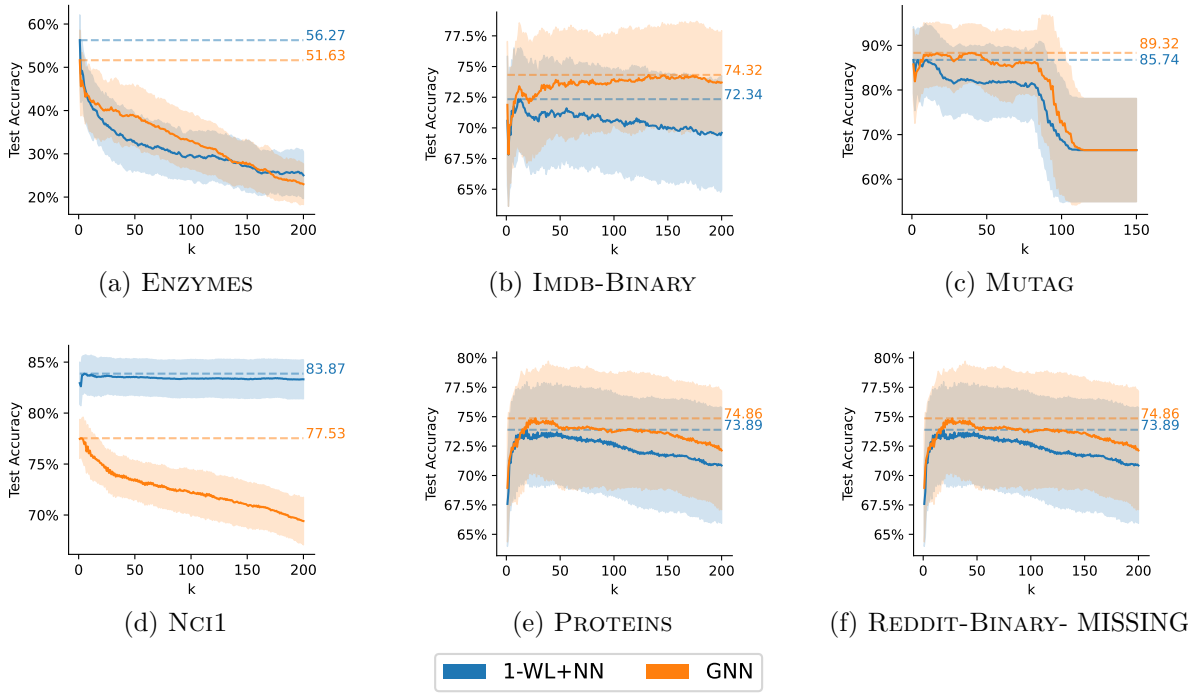

(a) ENZYMES (b) IMDB-BINARY (c) MUTAG

(d) NCI1 (e) PROTEINS (f) REDDIT-BINARY- MISSING

Figure 11.: Average classification accuracy achieved on each dataset by replacing the multilayer perceptron of the best-performing 1-WL+NN and GNN model with a classifier based on the k-nearest neighbors algorithm. We tested for different values of k.

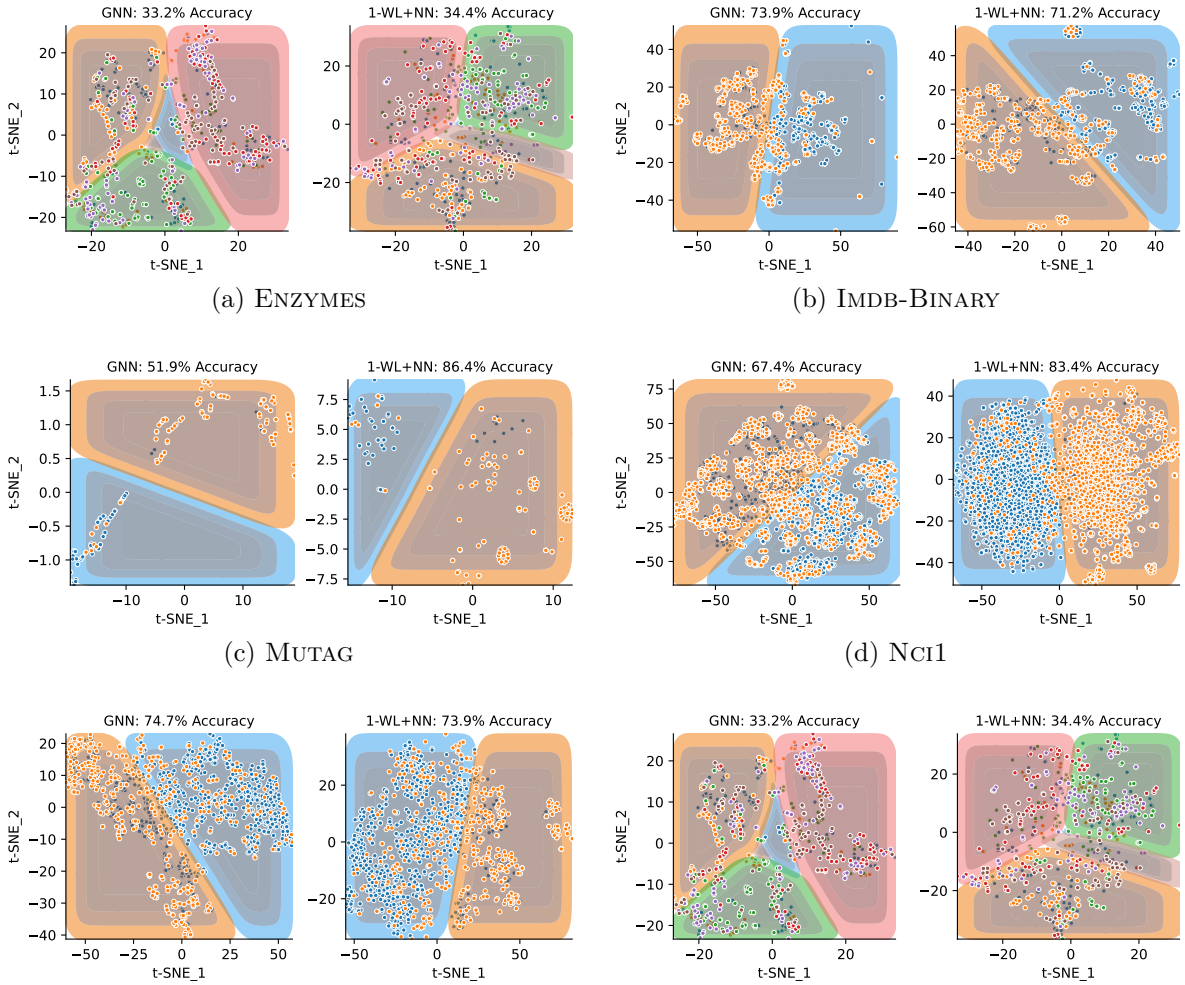

(a) Enzymes (b) Imdb-Binary

(c) Mutag (d) Nci1

(e) Proteins (f) Reddit-Binary- MISSING!

Figure 12.: Visualization of the decision boundary of each Support Vector Machine with a linear kernel using t-SNE.

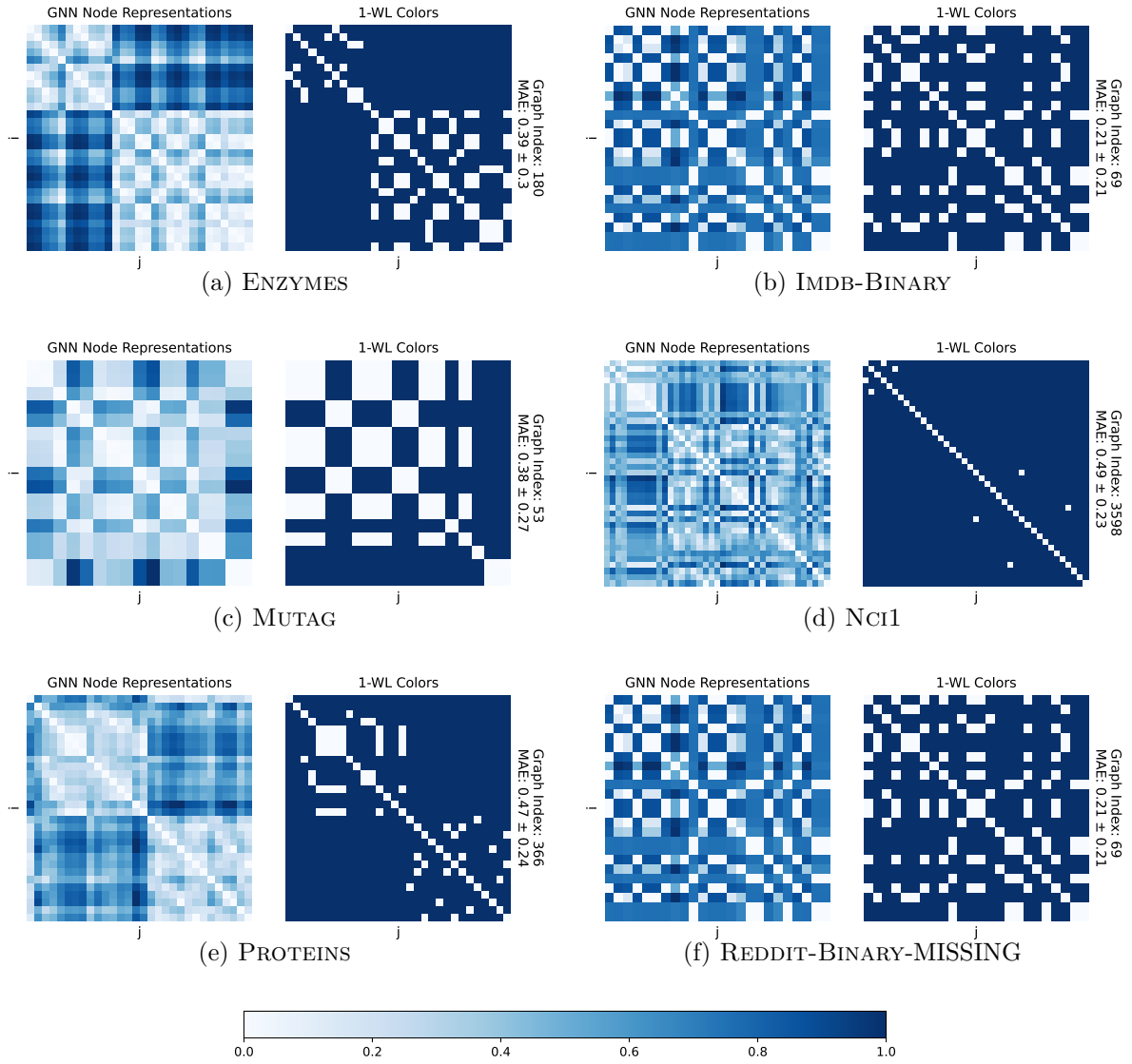

(a) Enzymes (b) Imdb-Binary

(c) Mutag (d) Nci1

(e) Proteins (f) Reddit-Binary-MISSING

Figure 13.: Visualizing the performance of the best-performing GNN models of each dataset in approximating node colors computed by the 1-WL algorithm. Here we randomly sampled a single graph for each dataset and visualized the approximation performance. For each calculation of the 1-WL colors, we utilized the number of iterations of the 1-WL algorithm to be the same as the best-performing 1-WL+NN model of each dataset. Specifically, this was 1 for all datasets except for Nci1, where it was 3.

Property	Dataset					
	ENZYMES	IMDB-BINARY	MUTAG	NCI1	PROTEINS	REDDIT-BINARY
MAE	0.49 ±0.3	0.14 ±0.15	0.42 ±0.29	0.42 ±0.22	0.49 ±0.26	
Number of 1-WL colors	230	64	32	27252	296	

Table 9.: MAE of the approximation performance of the best-perfoming GNN in relation to the number of unique 1-WL colors for each dataset. In particular, in comparison to the colors computed by the 1-WL alogrithm with a single iteration.

	Epsilon	Dataset					
		ENZYMES	IMDB-BINARY	MUTAG	NCI1	PROTEINS	REDDIT-BINARY
F1-Score	$\epsilon = 0.001$	52.55	60.97	62.01			
	$\epsilon = 0.01$	54.63	60.97	62.01			
	$\epsilon = 0.05$	62.33	71.68	62.01			
	$\epsilon = 0.1$	70.45	78.66	62.01			
	Number of 1-WL colors	230	64	32	27252	296	

Table 10.: MAE of the approximation performance of the best-perfoming GNN in relation to the number of unique 1-WL colors for each dataset. In particular, in comparison to the colors computed by the 1-WL alogrithm with a single iteration.

Bibliography

[1] R. Abboud, I. I. Ceylan, M. Grohe, and T. Lukasiewicz. The surprising power of graph neural networks with random node initialization. *arXiv preprint arXiv:2010.01179*, 2020.

[2] J. Atwood and D. Towsley. Diffusion-convolutional neural networks. *Advances in neural information processing systems*, 29, 2016.

[3] L. Babai. Lectures on graph isomorphism. University of Toronto, Department of Computer Science. Mimeographed lecture notes, October 1979, 1979.

[4] L. Babai. Graph isomorphism in quasipolynomial time. In *ACM SIGACT Symposium on Theory of Computing*, pages 684–697, 2016.

[5] L. Babai and L. Kucera. Canonical labelling of graphs in linear average time. In *Symposium on Foundations of Computer Science*, pages 39–46, 1979.

[6] D. Beaini, S. Passaro, V. Létourneau, W. Hamilton, G. Corso, and P. Liò. Directional graph networks. In *International Conference on Machine Learning*, pages 748–758. PMLR, 2021.

[7] K. M. Borgwardt, C. S. Ong, S. Schönauer, S. Vishwanathan, A. J. Smola, and H.-P. Kriegel. Protein function prediction via graph kernels. *Bioinformatics*, 21(suppl_1):i47–i56, 2005.

[8] X. Bresson and T. Laurent. A two-step graph convolutional decoder for molecule generation. *arXiv preprint arXiv:1906.03412*, 2019.

[9] T. Brown, B. Mann, N. Ryder, M. Subbiah, J. D. Kaplan, P. Dhariwal, A. Neelakantan, P. Shyam, G. Sastry, A. Askell, et al. Language models are few-shot learners. *Advances in neural information processing systems*, 33:1877–1901, 2020.

[10] J. Bruna, W. Zaremba, A. Szlam, and Y. LeCun. Spectral networks and locally connected networks on graphs. *arXiv preprint arXiv:1312.6203*, 2013.

[11] J. Cai, M. Fürer, and N. Immerman. An optimal lower bound on the number of variables for graph identifications. *Combinatorica*, 12(4):389–410, 1992.

[12] A. Cardon and M. Crochemore. Partitioning a graph in $O(|A| \log_2 |V|)$. *Theoretical Computer Science*, 19(1):85 – 98, 1982.

[13] G. Chen, P. Chen, C.-Y. Hsieh, C.-K. Lee, B. Liao, R. Liao, W. Liu, J. Qiu, Q. Sun, J. Tang, et al. Alchemy: A quantum chemistry dataset for benchmarking ai models. *arXiv preprint arXiv:1906.09427*, 2019.

[14] Z. Chen, S. Villar, L. Chen, and J. Bruna. On the equivalence between graph isomorphism testing and function approximation with GNNs. In *Advances in Neural Information Processing Systems*, pages 15868–15876, 2019.

[15] A. K. Debnath, R. L. Lopez de Compadre, G. Debnath, A. J. Shusterman, and C. Hansch. Structure-activity relationship of mutagenic aromatic and heteroaromatic nitro compounds. correlation with molecular orbital energies and hydrophobicity. *Journal of medicinal chemistry*, 34(2):786–797, 1991.

[16] M. Defferrard, X. Bresson, and P. Vandergheynst. Convolutional neural networks on graphs with fast localized spectral filtering. *Advances in neural information processing systems*, 29, 2016.

[17] D. K. Duvenaud, D. Maclaurin, J. Iparraguirre, R. Bombarell, T. Hirzel, A. Aspuru-Guzik, and R. P. Adams. Convolutional networks on graphs for learning molecular fingerprints. *Advances in neural information processing systems*, 28, 2015.

[18] F. Geerts. The expressive power of kth-order invariant graph networks, 2020.

[19] J. Gilmer, S. S. Schoenholz, P. F. Riley, O. Vinyals, and G. E. Dahl. Neural message passing for quantum chemistry. In *International Conference on Machine Learning*, 2017.

[20] M. Grohe. *Descriptive Complexity, Canonisation, and Definable Graph Structure Theory.* Lecture Notes in Logic. Cambridge University Press, 2017.

[21] W. L. Hamilton, R. Ying, and J. Leskovec. Inductive representation learning on large graphs. In *Advances in Neural Information Processing Systems*, pages 1025–1035, 2017.

[22] K. He, X. Zhang, S. Ren, and J. Sun. Deep residual learning for image recognition. In *Proceedings of the IEEE conference on computer vision and pattern recognition*, pages 770–778, 2016.

[23] K. Hornik. Approximation capabilities of multilayer feedforward networks. *Neural networks*, 4(2):251–257, 1991.

[24] N. Immerman and E. Lander. *Describing Graphs: A First-Order Approach to Graph Canonization*, pages 59–81. Springer, 1990.

[25] J. J. Irwin, T. Sterling, M. M. Mysinger, E. S. Bolstad, and R. G. Coleman. Zinc: a free tool to discover chemistry for biology. *Journal of chemical information and modeling*, 52 (7):1757–1768, 2012.

[26] T. N. Kipf and M. Welling. Semi-supervised classification with graph convolutional networks. In *International Conference on Learning Representations*, 2017.

[27] A. Krizhevsky, G. Hinton, et al. Learning multiple layers of features from tiny images. 2009.

[28] Y. Li, D. Tarlow, M. Brockschmidt, and R. Zemel. Gated graph sequence neural networks. *arXiv preprint arXiv:1511.05493*, 2015.

[29] R. Liu, S. Cantürk, F. Wenkel, S. McGuire, X. Wang, A. Little, L. O'Bray, M. Perlmutter, B. Rieck, M. Hirn, et al. Taxonomy of benchmarks in graph representation learning. In *Learning on Graphs Conference*, pages 6–1. PMLR, 2022.

[30] A. Micheli. Neural network for graphs: A contextual constructive approach. *IEEE Transactions on Neural Networks*, 20(3):498–511, 2009.

[31] C. Morris, N. M. Kriege, K. Kersting, and P. Mutzel. Faster kernel for graphs with continuous attributes via hashing. In *IEEE International Conference on Data Mining*, pages 1095–1100, 2016.

[32] C. Morris, M. Ritzert, M. Fey, W. L. Hamilton, J. E. Lenssen, G. Rattan, and M. Grohe. Weisfeiler and Leman go neural: Higher-order graph neural networks. In *AAAI Conference on Artificial Intelligence*, pages 4602–4609, 2019.

[33] C. Morris, N. M. Kriege, F. Bause, K. Kersting, P. Mutzel, and M. Neumann. TUDataset: A collection of benchmark datasets for learning with graphs. *CoRR*, 2020.

[34] C. Morris, G. Rattan, S. Kiefer, and S. Ravanbakhsh. Speqnets: Sparsity-aware permutation-equivariant graph networks. In *International Conference on Machine Learning*, pages 16017–16042. PMLR, 2022.

[35] G. Nikolentzos, M. Chatzianastasis, and M. Vazirgiannis. What do gnns actually learn? towards understanding their representations. *arXiv preprint arXiv:2304.10851*, 2023a.

[36] G. Nikolentzos, M. Chatzianastasis, and M. Vazirgiannis. Weisfeiler and leman go hyperbolic: Learning distance preserving node representations. In *International Conference on Artificial Intelligence and Statistics*, pages 1037–1054. PMLR, 2023b.

[37] R. Paige and R. Tarjan. Three partition refinement algorithms. *SIAM Journal on Computing*, 16(6):973–989, 1987.

[38] A. Radford, J. Wu, R. Child, D. Luan, D. Amodei, I. Sutskever, et al. Language models are unsupervised multitask learners. *OpenAI blog*, 1(8):9, 2019.

[39] R. Sato, M. Yamada, and H. Kashima. Random features strengthen graph neural networks. In *Proceedings of the 2021 SIAM International Conference on Data Mining (SDM)*, pages 333–341. SIAM, 2021.

[40] F. Scarselli, M. Gori, A. C. Tsoi, M. Hagenbuchner, and G. Monfardini. The graph neural network model. *IEEE transactions on neural networks*, 20(1):61–80, 2008.

[41] F. Scarselli, M. Gori, A. C. Tsoi, M. Hagenbuchner, and G. Monfardini. The graph neural network model. *IEEE Transactions on Neural Networks*, 20(1):61–80, 2009.

[42] N. Shervashidze, P. Schweitzer, E. J. Van Leeuwen, K. Mehlhorn, and K. M. Borgwardt. Weisfeiler-lehman graph kernels. *Journal of Machine Learning Research*, 12(9), 2011.

[43] A. Sperduti and A. Starita. Supervised neural networks for the classification of structures. *IEEE Transactions on Neural Networks*, 8(3):714–735, 1997.

[44] P. Veličković, G. Cucurull, A. Casanova, A. Romero, P. Lio, and Y. Bengio. Graph attention networks. *arXiv preprint arXiv:1710.10903*, 2017.

[45] C. Vignac, A. Loukas, and P. Frossard. Building powerful and equivariant graph neural networks with structural message-passing. *Advances in neural information processing systems*, 33:14143–14155, 2020.

[46] O. Vinyals, S. Bengio, and M. Kudlur. Order matters: Sequence to sequence for sets. *arXiv preprint arXiv:1511.06391*, 2015.

[47] N. Wale, I. A. Watson, and G. Karypis. Comparison of descriptor spaces for chemical compound retrieval and classification. *Knowledge and Information Systems*, 14:347–375, 2008.

[48] B. Weisfeiler and A. Leman. The reduction of a graph to canonical form and the algebra which appears therein. *Nauchno-Technicheskaya Informatsia*, 2(9):12–16, 1968.

[49] K. Xu, W. Hu, J. Leskovec, and S. Jegelka. How powerful are graph neural networks? In *International Conference on Learning Representations*, 2019.

[50] P. Yanardag and S. Vishwanathan. Deep graph kernels. In *Proceedings of the 21th ACM SIGKDD international conference on knowledge discovery and data mining*, pages 1365–1374, 2015.

[51] Z. Ying, J. You, C. Morris, X. Ren, W. Hamilton, and J. Leskovec. Hierarchical graph representation learning with differentiable pooling. *Advances in neural information processing systems*, 31, 2018.

[52] M. Zhang, Z. Cui, M. Neumann, and Y. Chen. An end-to-end deep learning architecture for graph classification. In *Proceedings of the AAAI conference on artificial intelligence*, volume 32, 2018.

[53] B. Zoph, V. Vasudevan, J. Shlens, and Q. V. Le. Learning transferable architectures for scalable image recognition. In *Proceedings of the IEEE conference on computer vision and pattern recognition*, pages 8697–8710, 2018.

A. Appendix Part I

1. Theoretical Connection

1.1. Lemma 19: Composition Lemma for 1-WL+NN

Before we begin with the actual composition proof, we give a formal definition and notation for multilayer perceptrons.

Definition 27 (Multilayer Perceptron)**.** Multilayer perceptrons are a class of functions from $\mathbb{R}^n$ to $\mathbb{R}^m$, with $n, m \in \mathbb{N}$. In this thesis, we define a multilayer perceptron as a finite sequence, such that a multilayer perceptron MLP is defined as $\mathsf{MLP} \coloneqq (\mathsf{MLP})_{i \in [T]}$ where T is the number of layers. For every $i \in [T]$, the i.th layer of the MLP is the i.th item in the finite sequence $(\mathsf{MLP})_i$. Further, all layers are recursively defined on any input v as:

$$\begin{aligned}(\mathsf{MLP})_0(v) &\coloneqq v \\ (\mathsf{MLP})_{i+1}(v) &\coloneqq \sigma_i(W_i \cdot (\mathsf{MLP})_i(v) + b_i), \quad \forall i \in [k-1]\end{aligned}$$

where σ_i is an element wise activation function, W_i is the weight matrix and b_i the bias vector of layer i. Note, that for each W_i, the succeeding W_{i+1} must have the same number of columns as W_i has rows, in order to be well-defined. Similarly, for every layer i, W_i and b_i have to have the same number of rows. Following this definition, when applying a MLP on an input $v \in \mathbb{R}^n$ it is defined as $\mathsf{MLP}(v) \coloneqq (\mathsf{MLP})_k(v)$.

Having established a formal definition and notation, we will now proof the 1-WL+NN composition lemma.

Proof of Lemma 19. Let $\mathcal{C}$ be a collection of functions computed by 1-WL+NN, $h_1, \ldots, h_n \in \mathcal{C}$, and $\mathsf{MLP}^\bullet$ a multilayer perceptron. Further, let $f_1, \ldots, f_n$ be the encoding functions, as well as $\mathrm{MLP}_1, \ldots, \mathrm{MLP}_n$ be the multilayer perceptrons used by $h_1, \ldots h_n$ respectively. As outlined in Figure 5, we will now construct f^* and MLP^*, such that for all graphs $G \in \mathcal{X}$:

$$\mathsf{MLP}^\bullet(h_1(G), \ldots, h_n(G)) = \mathsf{MLP}^* \circ f^*(\{\!\{\text{1-WL}(G)(v) \mid v \in V(G)\}\!\}),$$

with which we can conclude that the composition of multiple functions computable by 1-WL+NN, is also 1-WL+NN computable.

We define the new encoding function f^* to work as follows on an arbitrary input multiset M:

$$f^*(M) \coloneqq \mathsf{concat}(\begin{bmatrix} f_1(M) \\ \vdots \\ f_n(M) \end{bmatrix}),$$

where concat is the concatenation function, concatenating all encoding vectors to one single vector.

Using the decomposition introduced in Definition 27, we can decompose each MLP_i for $i \in [n]$ at layer $j > 0$ as follows: $(\mathsf{MLP}_i)_j(v) := \sigma_{i,j}(W_j^i \cdot (\mathsf{MLP}_i)_{j-1}(v) + b_j^i)$. Using this notation we construct MLP^* as follows:

$$
\begin{aligned}
(\mathsf{MLP}^*)_0(v) &:= v \\
(\mathsf{MLP}^*)_{j+1}(v) &:= \sigma_j^*(W_j^* \cdot (\mathsf{MLP}^*)_j(v) + \mathsf{concat}(\begin{bmatrix} b_j^1 \\ \vdots \\ b_j^n \end{bmatrix})) && ,\forall j \in [T-1] \\
(\mathsf{MLP}^*)_{j+T+1}(v) &:= (\mathsf{MLP}^\bullet)_{j+1}(v) && ,\forall j \in [T^\bullet - 1]
\end{aligned}
$$

where T is the maximum number of layers of the set of MLP_i's, and $T^\bullet$ is the number of layers of the given $\mathsf{MLP}^\bullet$. Thereby, we define in the first equation the start of the sequence as the input; with the second line, we construct the "simultaneous" execution of the MLP_i's, and in the last equation line, we add the layers of the given $\mathsf{MLP}^\bullet$ to the end. Further, we define the weight matrix W_j^* as follows:

$$
W_j^* := \begin{bmatrix} W_j^1 & 0 & \dots & 0 \\ 0 & W_j^2 & \ddots & \vdots \\ \vdots & \ddots & \ddots & 0 \\ 0 & \dots & 0 & W_j^n \end{bmatrix},
$$

such that we build a new matrix where each individual weight matrix is placed along the diagonal. Here we denote with "0" zero matrices with the correct dimensions, such that W_j^* is well-defined. Important to note, should for an MLP_i, W_j^i not exist, because it has less than j layers, we use for W_j^i the identity matrix I_m where m is the dimension of the output computed by MLP_i. And finally, we define the overall activation function σ_j^* as following:

$$
\sigma_j^*(v) := \begin{bmatrix} \sigma_{1,j}(v[1]) \\ \vdots \\ \sigma_{1,j}(v[d_1]) \\ \cdot \\ \cdot \\ \cdot \\ \cdot \\ \cdot \\ \sigma_{n,j}(v[d_1 + \dots + d_{n-1} + 1]) \\ \vdots \\ \sigma_{n,j}(v[d_1 + \dots + d_n]) \end{bmatrix},
$$

where d_i is the dimension of the output of MLP_i at layer j, and for the ease of readability we denote the i.th component of vector v here with $v[i]$. Thereby, we construct an activation function that applies each respective activation function of the MLP_i's individually to their respective computation. □

1.2. Theorem 14: Continuous Case: "GNN $\subseteq$ 1-WL+NN"

We will prove Theorem 14 by introducing a definition and then two lemmas using that definition, collectively proving the entire theorem. In particular, we define the property that a collection

of functions is able to find any $\simeq_{1\text{WL}}$ equivalence class. In the subsequent Lemma 29, we will show that the quality of 1-WL-Discriminating of a collection implies the ability to locate any $\simeq_{1\text{WL}}$-equivalence class. Finally, with Lemma 30, that this quality further implies the capability of being GNN-Approximating. The overall proof is inspired by the work of [14].

For this proof, we make the major assumption that a continuous 1-WL algorithm exists that operates over continuous values.

Definition 28 (Locating $\simeq_{1\text{WL}}$-Equivalence Classes)**.** Let $\mathcal{C}$ be a collection of continuous functions from $\mathcal{X}$ to $\mathbb{R}$. If for all $\epsilon \in \mathbb{R}$ with $\epsilon > 0$ and for every graph $G^* \in \mathcal{X}$ the function h_{G^*} exists in $\mathcal{C}$, with the following properties:

1. for all $G \in \mathcal{X} : h_{G^*}(G) \geq 0$,
2. for all $G \in \mathcal{X}$ with $G \simeq_{1\text{WL}} G^* : h_{G^*}(G) = 0$, and
3. there exists a constant $\delta_{G^*} > 0$, such that for all $G \in \mathcal{X}$ with $h_{G^*}(G) < \delta_{G^*}$ there exists a graph $G' \in \mathcal{X}/\simeq_{1\text{WL}}(G)$ in the equivalence class of G such that $\|G' - G^*\|_2 < \epsilon$

we say $\mathcal{C}$ is able to locate every $\simeq_{1\text{WL}}$ equivalence class.

One can interpret this function h_{G^*} as a kind of loss function that measures the similarity between its input graph to G^*. It yields no loss for the input G, if G is indistinguishable from G^* by the 1-WL algorithm ($G \simeq_{1\text{WL}} G^*$), only a small loss if G is close to a graph in the $\simeq_{1\text{WL}}$ equivalence class of G^* (the loss is upper bounded by δ_{G^*}), and an arbitrary loss otherwise.

Lemma 29. Let $\mathcal{C}$ be a collection of continuous functions from $\mathcal{X}$ to $\mathbb{R}$ computable by 1-WL+NN. If $\mathcal{C}$ is 1-WL-Discriminating, then there exists a collection of functions $\mathcal{C}'$ computable by 1-WL+NN that is able to locate every $\simeq_{1\text{WL}}$ equivalence class on $\mathcal{X}$.

Proof. Let $G^* \in \mathcal{X}$ be fixed and $\epsilon > 0$ be given. Since $\mathcal{C}$ is 1-WL-Discriminating, we know that for every $G \in \mathcal{X}$ with $G \not\simeq_{1\text{WL}} G^*$, there exists a function $h_{G,G^*} \in \mathcal{C}$ such that $h_{G,G^*}(G) \neq h_{G,G^*}(G^*)$. We use this property to construct for each $G \in \mathcal{X}$ with $G \not\simeq_{1\text{WL}} G^*$ a set A_{G,G^*} as follows:

$$A_{G,G^*} \coloneqq \{G' \in \mathcal{X} \mid h_{G,G^*}(G') \in (h_{G,G^*}(G) \pm \frac{|h_{G,G^*}(G) - h_{G,G^*}(G^*)|}{2})\},$$

where $(a \pm b)$ is the open set $(a - b, a + b)$ over $\mathbb{R}$. One can use Figure A.1 below for a better understanding, when a graph G' is contained in A_{G,G^*} and when not. With the illustration one can easily see, that $G \in A_{G,G^*}$ and $G^* \notin A_{G,G^*}$.

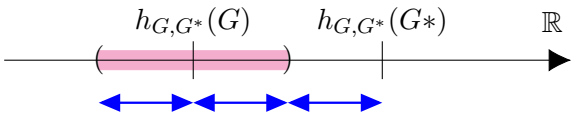

Figure A.1.: An illustration to better understand the proof. The set A_{G,G^*} consists of all graphs G that are mapped by h_{G,G^*} into the pink area, which size depends on the distance between the image of G and G^* under h_{G,G^*}. Moreover, the blue distances all have the same length.

Furthermore, by assumption h_{G,G^*} is continuous, such that A_{G,G^*} is an open set. For every $G \in \mathcal{X}$ with $G \simeq_{1\text{WL}} G^*$ we define A_{G,G^*} as follows:

$$A_{G,G^*} \coloneqq \{G' \in \mathcal{X} \mid \|G' - G\|_2 < \epsilon\},$$

where $\|\cdot\|_2$ is the l_2 norm.

Thus, $\{A_{G,G^*}\}_{G\in\mathcal{X}}$ is an open cover of $\mathcal{X}$. Since $\mathcal{X}$ is compact, there exists a finite subset $\mathcal{X}_0$ such that $\{A_{G,G^*}\}_{G\in\mathcal{X}_0}$ also covers $\mathcal{X}$. Hence, $\forall G \in \mathcal{X} \exists G_0 \in \mathcal{X}_0 : G \in A_{G_0,G^*}$.

We define the desired function h_{G^*} as follows:

$$h_{G^*}(\cdot) = \sum_{\substack{G_0\in\mathcal{X}_0 \\ G_0\not\simeq_{1\text{WL}}G^*}} \overline{h}_{G_0,G^*}(\cdot), \tag{A.1}$$

where we define $\overline{h}_{G_0,G^*}$ almost exactly the same as in a previous proof:

$$\begin{aligned}\overline{h}_{G_0,G^*}(\cdot) &= |h_{G_0,G^*}(\cdot) - h_{G_0,G^*}(G^*)| &\text{(A.2)}\\ &= \max(h_{G_0,G^*}(\cdot) - h_{G_0,G^*}(G^*)) + \max(h_{G_0,G^*}(G^*) - h_{G_0,G^*}(\cdot)) &\text{(A.3)}\end{aligned}$$

Note that, "$h_{G_0,G^*}(G^*)$" is a constant in the definition of $\overline{h}_{G_0,G^*}(\cdot)$. We will shortly proof, that $h_{G^*}(\cdot)$ fulfills the desired properties on input $G \in \mathcal{X}$:

1. By construction, any $\overline{h}_{G_0,G^*}$ is non-negative, such that the sum over these functions is also non-negative.
2. If $G \simeq_{1\text{WL}} G^*$, using Lemma 17 we know that $h_{G^*}(G) = h_{G^*}(G^*)$, and by definition $h_{G^*}(G^*) = 0$, such that we can conclude $h_{G^*}(G) = 0$.
3. Let δ_{G^*} be:
$$\delta_{G^*} \coloneqq \frac{1}{2} \min_{\substack{G_0\in\mathcal{X} \\ G_0\not\simeq_{1\text{WL}}G^*}} |h_{G_0,G^*}(G_0) - h_{G_0,G^*}(G^*)|.$$
Prove by contraposition: Assume that for every graph $G' \in \mathcal{X}/\simeq_{1\text{WL}}(G)$: $\|G' - G^*\|_2 \geq \epsilon$. Hence, $G \notin \bigcup_{G'\in\mathcal{X}/\simeq_{1\text{WL}}(G^*)} A_{G',G^*}$ (not in the union of l_2 balls of size ϵ around all graphs of the equivalence class of G^*). However, since $\{A_{G,G^*}\}_{G\in\mathcal{X}_0}$ is a cover of $\mathcal{X}$, there must exist a $G_0 \in \mathcal{X}_0$ with $G_0 \not\simeq_{1\text{WL}} G^*$ such that $G \in A_{G_0,G^*}$. Thus, by definition of A_{G_0,G^*} we know that $h_{G_0,G^*}(G) \in (h_{G_0,G^*}(G_0) \pm \frac{|h_{G_0,G^*}(G_0) - h_{G_0,G^*}(G^*)|}{2})$, which when reformulated states:
$$|h_{G_0,G^*}(G) - h_{G_0,G^*}(G_0)| < \frac{1}{2}|h_{G_0,G_0}(G) - h_{G_0,G^*}(G^*)|. \tag{A.4}$$
Using this, we can prove $\overline{h}_{G_0,G^*}(G) \geq \delta_{G^*}$, which implies $h_{G^*}(G) \geq \delta_{G^*}$ and concludes the proof:
$$\begin{aligned}\overline{h}_{G_0,G^*}(G) &= |h_{G_0,G^*}(G) - h_{G_0,G^*}(G^*)| \\ &\geq |h_{G_0,G^*}(G_0) - h_{G_0,G^*}(G^*)| - |h_{G_0,G^*}(G) - h_{G_0,G^*}(G_0)| &\text{(A.5)}\\ &\geq \frac{1}{2}|h_{G_0,G^*}(G_0) - h_{G_0,G^*}(G^*)| &\text{(A.6)}\\ &\geq \frac{1}{2} \min_{\substack{G_0\in\mathcal{X} \\ G_0\not\simeq_{1\text{WL}}G^*}} |h_{G_0,G^*}(G_0) - h_{G_0,G^*}(G^*)| =: \delta_{G^*}\end{aligned}$$
To understand these inequalities, it helps to visualize them, hence see Figure A.2. We will try to give an explanation now, using the colored distances depicted in Figure A.2. In Equation (A.5), we use the fact that the red distance is always greater than the green minus the blue distance. Further, using Equation (A.4), we know that the blue distance is always smaller than half of than the green distance. Using this fact, it is easy to see

that in Equation (A.6) the green minus the blue distance is always greater than or equal to the half of the green distance.

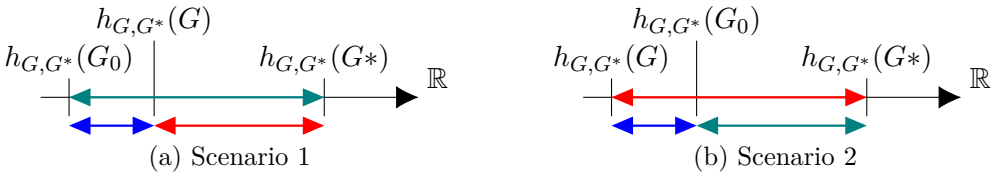

(a) Scenario 1 (b) Scenario 2

Figure A.2.: An illustration of two general scenarios to better understand the above used inequalities. Note that, there exists two more general scenarios, with $h_{G_0,G^*}(G^*) < h_{G_0,G^*}(G_0)$, but since we use the absolute function as our measure of distance, these scenarios are equivalent to the ones depicted due to the symmetry of the absolute function. In Table A.1 below, we listed all colors used to decode the distances in the figures with their corresponding term in the inequalities.

Color	**Term**
red	$\lvert h_{G_0,G^*}(G) - h_{G_0,G^*}(G^*)\rvert$
green	$\lvert h_{G_0,G^*}(G_0) - h_{G_0,G^*}(G^*)\rvert$
blue	$\lvert h_{G_0,G^*}(G) - h_{G_0,G^*}(G_0)\rvert$

Table A.1.: Color legend for the proof of Lemma 29 and Figure A.2.

Consequently, we know that if $h_{G^*}(G) < \delta_G$ it means that $G \in \bigcup_{G' \in \mathcal{X}/\simeq_{1\text{WL}}(G^*)} A_{G',G^*}$, which implies that there exists $G' \in \mathcal{X}/\simeq_{1\text{WL}}(G)$ with $\|G' - G^*\|_2 < \epsilon$.

As a final note, we can construct a multilayer perceptron $\mathsf{MLP}_{h_{G^*}}$ computing the function $h_{G^*}(\cdot)$ as in Equation (A.1). The $\mathsf{MLP}_{h_{G^*}}$ gets as input a vector of the output of the finite set of functions $\{\overline{h}_{G_0,G^*}\}_{G_0 \in \mathcal{X}_0,\ G_0 \not\simeq_{1\text{WL}} G^*}$ applied on the input graph. Further, Equation (A.1) can be encoded by replacing the max operator by the non-linear activation function ReLU. Using Lemma 19, we can conclude that $h_{G^*}(\cdot)$ is computable by 1-WL+NN.

□

Lemma 30. Let $\mathcal{C}$ be a collection of continuous functions from $\mathcal{X}$ to $\mathbb{R}$ computable by 1-WL+NN. If $\mathcal{C}$ is able to locate every $\simeq_{1\text{WL}}$ equivalence class on $\mathcal{X}$, then there exists a collection of functions $\mathcal{C}'$ computable by 1-WL+NN that is GNN-Approximating.

Proof. Let $\mathcal{A}$ be a continuous function from $\mathcal{X}$ to $\mathbb{R}$ computable by a GNN. Since $\mathcal{X}$ is compact, this implies that $\mathcal{A}$ is uniformaly continuous on $\mathcal{X}$, which further implies that $\forall \epsilon > 0 \exists r > 0$ such that $\forall G_1, G_2 \in \mathcal{X}$, if $\|G_1 - G_2\|_2 < r$, then $|\mathcal{A}(G_1) - \mathcal{A}(G_2)| < \epsilon$. Further, since $\mathcal{A}$ is GNN computable, we know that $\forall G_1, G_2 \in \mathcal{X}$, if $G_1 \simeq_{1\text{WL}} G_2 : \mathcal{A}(G_1) = \mathcal{A}(G_2)$, hence if $G' \in \mathcal{X}/\simeq_{1\text{WL}}(G_1)$ with $\|G' - G_2\|_2 < r$ exists, than $|\mathcal{A}(G_1) - \mathcal{A}(G_2)| < \epsilon$.

Throughout the rest of the proof, let $\epsilon > 0$ be fixed. Using the property described above, we know that for this ϵ there exists a constant r, which we will fix for the remainder of the proof as well. Further, by the assumptions of the lemma we try to prove, we know that for any $\epsilon' > 0$ there exists $h_G \in \mathcal{C}$ for any $G \in \mathcal{X}$ with the above described properties. We choose $\epsilon' := r$ for

all $h_G \in \mathcal{C}$ throughout the proof.

For any $G \in \mathcal{X}$, we define the set $h_G^{-1}(a) \coloneqq \{G' \in \mathcal{X} \mid h_G(G') \in [0, a)\}$, as the set of graphs that are mapped into the open interval $[0, a)$ by h_G. We illustrated this set in Figure A.3 for a better understanding.

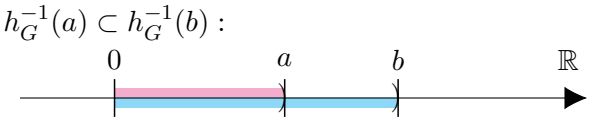

Figure A.3.: Illustration of the set $h_G^{-1}(\cdot)$ for two arbitrary values a, b with $a < b$. The pink area visualizes the open interval $[0, a)$, and similarly in blue for $[0, b)$.

Then, by definition of h_G, there exists a constant δ_G such that:

$$h_G^{-1}(\delta_G) \subseteq \bigcup_{G' \in \mathcal{X}/\simeq_{1\text{WL}}(G)} \{G'' \in \mathcal{X} \mid \|G'' - G'\|_2 < r\}.$$

Since h_G is continuous by definition, $h_G^{-1}(\delta_G)$ is an open set. Hence, $\{h_G^{-1}(\delta_G)\}_{G \in \mathcal{X}}$ is an open cover of $\mathcal{X}$, and further as $\mathcal{X}$ is compact, there exists a finite subset $\mathcal{X}_0 \subseteq \mathcal{X}$ such that $\{h_{G_0}^{-1}(\delta_{G_0})\}_{G_0 \in \mathcal{X}_0}$ is also a cover of $\mathcal{X}$. For each $G_0 \in \mathcal{X}_0$, we construct the function φ_{G_0} from $\mathcal{X}$ to $\mathbb{R}$ as follows:

$$\varphi_{G_0}(\cdot) \coloneqq \max(\delta_{G_0} - h_{G_0}(\cdot),\ 0).$$

The function has two important properties, for once it is non-negative and for any $G \in \mathcal{X}$: $\varphi_{G_0}(G) > 0$, if and only if $G \in h_{G_0}^{-1}(\delta_{G_0})$, thereby acting as a sort of weak indicator function. Building up on this property, we construct for each $G_0 \in \mathcal{X}_0$ the function ψ_{G_0} from $\mathcal{X}$ to $\mathbb{R}$ as follows:

$$\psi_{G_0}(\cdot) \coloneqq \frac{\varphi_{G_0(\cdot)}}{\sum_{G' \in G_0} \varphi_{G'}(\cdot)},$$

which is well-defined, because $\{h_{G_0}^{-1}(\delta_{G_0})\}_{G_0 \in \mathcal{X}_0}$ is a cover of $\mathcal{X}$, such that we can conclude that for any input graph G on $\psi_{G_0}(\cdot)$ there exists a set $h_{G_0}^{-1}(\delta_{G_0})$ with $G \in h_{G_0}^{-1}(\delta_{G_0})$ implying $\varphi_{G_0}(G) > 0$, thus making the denominator not 0. The function ψ_{G_0} has two important properties, for once it is non-negative, because φ_G for all $G \in \mathcal{X}$ is non-negative, and for any $G \in \mathcal{X} : \psi_{G_0}(G) > 0$, if and only if $G \in h_{G_0}^{-1}(\delta_{G_0})$.

Further, we can observe that the set of functions $\{\psi_{G_0}\}_{G_0 \in \mathcal{X}_0}$ is a partition of unity on $\mathcal{X}$ with respect to the open cover $\{h_{G_0}^{-1}(\delta_{G_0})\}_{G_0 \in \mathcal{X}_0}$, because:

1. For any $G \in \mathcal{X}$ the set of functions mapping G not to 0 is finite, as the set of all functions $\{\psi_{G_0}\}_{G_0 \in \mathcal{X}_0}$ is finite, since $\mathcal{X}_0$ is finite.
2. For any $G \in \mathcal{X} : \sum_{G_0 \in \mathcal{X}_0} \psi_{G_0}(G) = 1$, since:

$$\sum_{G_0 \in \mathcal{X}_0} \psi_{G_0}(G) \ = \sum_{G_0 \in \mathcal{X}_0} \frac{\varphi_{G_0(G)}}{\sum_{G' \in \mathcal{X}_0} \varphi_{G'}(G)} = \frac{\sum_{G_0 \in \mathcal{X}_0} \varphi_{G_0(G)}}{\sum_{G' \in \mathcal{X}_0} \varphi_{G'}(G)} = 1.$$

We can use this property to decompose the given function $\mathcal{A}$ as follows on any input $G \in \mathcal{X}$:

$$\mathcal{A}(G) = \mathcal{A}(G) \cdot \Big(\sum_{G_0 \in \mathcal{X}_0} \psi_{G_0}(G) \Big) = \sum_{G_0 \in \mathcal{X}_0} \mathcal{A}(G) \cdot \psi_{G_0}(G).$$

Recall the property from the beginning of the proof that for any $G \in \mathcal{X}$ if $G \in h_{G_0}^{-1}(\delta_{G_0})$, then there exists a $G' \in \mathcal{X}/\simeq_{1\mathrm{WL}}(G)$ with $\|G' - G_0\|_2 < r$, which implies that $|\mathcal{A}(G) - \mathcal{A}(G_0)| < \epsilon$. With this, we can construct a function $\hat{\mathcal{A}}$ on $\mathcal{X}$ that approximates $\mathcal{A}$ within accuracy ϵ:

$$\hat{\mathcal{A}}(\cdot) = \sum_{G_0 \in \mathcal{X}_0} \mathcal{A}(G_0) \cdot \psi_{G_0}(\cdot).$$

Note that, "$\mathcal{A}(G_0)$" is a constant here. To prove that $\hat{\mathcal{A}}$ approximates $\mathcal{A}$ within accuracy ϵ we need to show that $\sup_{G \in \mathcal{X}} |\mathcal{A}(G) - \hat{\mathcal{A}}(G)| < \epsilon$. Let $G \in \mathcal{X}$ be arbitrary, then:

$$\begin{aligned}
|\mathcal{A}(G) - \hat{\mathcal{A}}(G)| &= \Big|\mathcal{A}(G) \cdot \Big(\sum_{G_0 \in \mathcal{X}_0} \cdot \psi_{G_0}(G)\Big) \; - \sum_{G_0 \in \mathcal{X}_0} \mathcal{A}(G_0) \cdot \psi_{G_0}(G)\Big| \\
&= \Big|\sum_{G_0 \in \mathcal{X}_0} \mathcal{A}(G) \cdot \psi_{G_0}(G) \; - \sum_{G_0 \in \mathcal{X}_0} \mathcal{A}(G_0) \cdot \psi_{G_0}(G)\Big| \\
&= \sum_{G_0 \in \mathcal{X}_0} |\mathcal{A}(G) - \mathcal{A}(G_0)| \cdot \psi_{G_0}(G) \\
&< \sum_{G_0 \in \mathcal{X}_0} \epsilon \cdot \psi_{G_0}(G) \qquad \text{(A.7)} \\
&= \epsilon \cdot \sum_{G_0 \in \mathcal{X}_0} \psi_{G_0}(G) \\
&= \epsilon \cdot 1
\end{aligned}$$

In Equation (A.7), we use the fact that applies to all $G_0 \in \mathcal{X}_0$ on input G:

- If $\psi_{G_0}(G) > 0$, than we know that $G \in h_{G_0}^{-1}(\delta_{G_0})$, such that we can upper bound $|\mathcal{A}(G) - \mathcal{A}(G_0)| < \epsilon$.
- If $\psi_{G_0}(G) = 0$, we know that the no matter what $|\mathcal{A}(G) - \mathcal{A}(G_0)|$ is, the summand is 0, such that we can just assume $|\mathcal{A}(G) - \mathcal{A}(G_0)| < \epsilon$ without loss of generality.

In the end, we give a short explanation, that $\hat{A}$ is computable by $\mathsf{1\text{-}WL{+}NN}$. For this we construct a multilayer perceptron with three layers and then conclude with Lemma 19 the computability. Let us therefore break down the whole construction of $\hat{\mathcal{A}}$:

$$\hat{\mathcal{A}}(\cdot) = \sum_{G_0 \in \mathcal{X}_0} \mathcal{A}(G_0) \cdot \frac{1}{\sum_{G' \in \mathcal{X}_0} \max(\delta_{G'} - h_{G'}(\cdot),\ 0)} \cdot \max(\delta_{G_0} - h_{G_0}(\cdot),\ 0).$$

We construct a multilayer perceptron $\mathsf{MLP}_{\hat{\mathcal{A}}}$ that takes in as input a vector of the output of the finite set of functions $\{h_{G_0}\}_{G_0 \in \mathcal{X}_0}$ applied on the input graph. In the first layer we compute each "$\max(\delta_{G_0} - h_{G_0}(\cdot))$" term, where δ_{G_0} is a constant, in particular the bias, and the max operator is replaced by the activation function ReLU. In the second layer, we compute the sum of the denominator of the fraction, to which we apply the activation function $f(x) \coloneqq \frac{1}{x}$. In the last layer we compute the overall sum where $\mathcal{A}(G_0)$ is a constant. □

B. Appendix Part II

1. Definitions

1.1. Definition of the normalized Shannon Index

We calculate the normalized Shannon index as follows:

$$-\frac{1}{\log_2(|C|)} \cdot \sum_{i \in C} \frac{n_i}{n} \cdot \log_2(\frac{n_i}{n}) \tag{B.1}$$

where n is the total number of samples of the dataset, C is the set of all classes, and n_i is the number of samples of the class $i \in C$. As an example, for the dataset PROTEINS the variables are set to be the following: $C = \{0, 1\}$ with $n_0 = 663$ and $n_1 = 450$, so that $n = 1113$, yielding a rounded value of 0.973.

1.2. Theoretical Maximum Accuracy Analysis

Table B.1.: An overview of the maximum theoretical classification accuracy achievable for each dataset based on the number of 1-WL iterations in percent. A hyphen "-" indicates that the maximum accuracy has converged with fewer iterations, implying that further iterations do not improve the accuracy. "OOM" denotes out of memory error.

	Datasets	Iterations of the 1-WL algorithm					
		0	1	2	3	4	5
Bioinformatics	DD	1.00	-	-	-	-	-
	ENZYMES	0.81	1.00	-	-	-	-
	KKI	1.00	-	-	-	-	-
	OHSU	1.00	-	-	-	-	-
	Peking_1	1.00	-	-	-	-	-
	PROTEINS	0.92	1.00	-	-	-	-
Small molecules	AIDS	1.00	1.00	-	-	-	-
	BZR	0.96	0.99	1.00	-	-	-
	COX2	0.93	0.96	0.99	1.00	-	-
	DHFR	0.92	0.95	1.00	1.00	-	-
	FRANKENSTEIN	0.63	0.77	0.88	0.89	0.89	-
	MUTAG	0.93	0.96	0.99	1.00	-	-
	NCI1	0.91	1.00	1.00	1.00	-	-
	NCI109	0.92	1.00	1.00	1.00	-	-
	PTC_MR	0.92	0.98	0.99	-	-	-
Social networks	COLLAB	0.61	0.98	-	-	-	-
	IMDB-BINARY	0.61	0.89	-	-	-	-
	IMDB-MULTI	0.44	0.63	-	-	-	-
	REDDIT-BINARY	0.84	1.00	-	-	-	-
	REDDIT-MULTI-5K	0.55	1.00	-	-	-	-
	REDDIT-MULTI-12K	0.36	OOM	OOM	OOM	OOM	OOM

1.3. Hyperparameter Configuration and Optimization

Table B.2.: 1-WL+NN!

Hyperparameter	Dataset					
	ENZYMES	IMDB-BINARY	MUTAG	NCI1	PROTEINS	REDDIT-BINARY
Batch Size	32	32	32	33	32	32
Learning Rate	$X \sim U(0.0001, 0.1)$	$X \sim U(0.0001, 0.1)$	$X \sim U(0.0001, 0.1)$	$X \sim U(0.0001, 0.1)$	$X \sim U(0.0001, 0.1)$	$X \sim U(0.0001, 0.1)$
Max Epochs	200	200	200	200	200	200
Optimizer	Adam	Adam	Adam	Adam	Adam	Adam
Scheduler	ReduceLROnPlateau	ReduceLROnPlateau	ReduceLROnPlateau	ReduceLROnPlateau	ReduceLROnPlateau	ReduceLROnPlateau
Number of 1-WL iterations	$\{1, 2, 3\}$	$\{1, 2, 3, 4\}$	$\{1, 2, 3, 4\}$	$\{1, 2, 3\}$	$\{1, 2, 3, 4\}$	$\{1, 2\}$
Use 1-WL-Convergence	False	False	False	False	False	False
MLP Activation Function	ReLU	ReLU	ReLU	ReLU	ReLU	ReLU
MLP Normalization	BatchNorm	BatchNorm	BatchNorm	BatchNorm	BatchNorm	BatchNorm
MLP Number of Layers	$\{2, 3, 4, 5\}$	$\{2, 3, 4, 5\}$	$\{2, 3, 4, 5\}$	$\{2, 3, 4, 5\}$	$\{2, 3, 4, 5\}$	$\{2, 3, 4, 5\}$
MLP Dropout	$X \sim U(0, 0.2)$	$X \sim U(0, 0.2)$	$X \sim U(0, 0.2)$	$X \sim U(0, 0.2)$	$X \sim U(0, 0.2)$	$X \sim U(0, 0.2)$
Embedding Dimension	$\{\text{None}, 16, 32, 64, 128\}$	$\{\text{None}, 16, 32, 64, 128\}$	$\{\text{None}, 16, 32, 64, 128\}$	$\{\text{None}, 16, 32, 64, 128\}$	$\{\text{None}, 16, 32, 64, 128\}$	$\{\text{None}, 16, 32, 64, 128\}$
Pooling function	{Max, Mean, Sum}	{Max, Mean, Sum}	{Max, Mean, Sum}	{Max, Mean, Sum}	{Max, Mean, Sum}	{Max, Mean, Sum}

Table B.3.: An Overview of hyperparameters we sweeped and tested each dataset with.

Hyperparameter	Dataset					
	ENZYMES	IMDB-BINARY	MUTAG	NCI1	PROTEINS	REDDIT-BINARY
Batch Size	32	32	32	$\{33, 129\}$	32	32
Learning Rate	$X \sim U(0.0001, 0.1)$	$X \sim U(0.0001, 0.1)$	$X \sim U(0.0001, 0.1)$	$X \sim U(0.0001, 0.1)$	$X \sim U(0.0001, 0.1)$	$X \sim U(0.0001, 0.1)$
Max Epochs	200	200	200	200	200	200
Optimizer	Adam	Adam	Adam	Adam	Adam	Adam
Scheduler	ReduceLROnPlateau	ReduceLROnPlateau	ReduceLROnPlateau	ReduceLROnPlateau	ReduceLROnPlateau	ReduceLROnPlateau
GNN Architecture	{GAT, GCN, GIN}	{GAT, GCN, GIN}	{GAT, GCN, GIN}	{GAT, GCN, GIN}	{GAT, GCN, GIN}	{GAT, GCN, GIN}
GNN Activation Function	ReLU	ReLU	ReLU	ReLU	ReLU	ReLU
GNN Dropout	$X \sim U(0, 0.2)$	$X \sim U(0, 0.2)$	$X \sim U(0, 0.2)$	$X \sim U(0, 0.2)$	$X \sim U(0, 0.2)$	$X \sim U(0, 0.2)$
GNN Hidden Dimension	$\{16, 32, 64, 128\}$	$\{16, 32, 64, 128\}$	$\{16, 32, 64, 128\}$	$\{16, 32, 64, 128\}$	$\{16, 32, 64, 128\}$	$\{16, 32, 64, 128\}$
GNN Jumping-Knowledge	cat	cat	cat	cat	cat	cat
GNN Number of Layers	5	5	5	5	5	5
MLP Activation Function	ReLU	ReLU	ReLU	ReLU	ReLU	ReLU
MLP Normalization	BatchNorm	BatchNorm	BatchNorm	BatchNorm	BatchNorm	BatchNorm
MLP Number of Layers	$\{2, 3, 4, 5\}$	$\{2, 3, 4, 5\}$	$\{2, 3, 4, 5\}$	$\{2, 3, 4, 5\}$	$\{2, 3, 4, 5\}$	$\{2, 3, 4, 5\}$
MLP Dropout	$X \sim U(0, 0.2)$	$X \sim U(0, 0.2)$	$X \sim U(0, 0.2)$	$X \sim U(0, 0.2)$	$X \sim U(0, 0.2)$	$X \sim U(0, 0.2)$
Pooling function	{Max, Mean, Sum}	{Max, Mean, Sum}	{Max, Mean, Sum}	{Max, Mean, Sum}	{Max, Mean, Sum}	{Max, Mean, Sum}

Table B.4.: 1-WL+NN!

Hyperparameter	Dataset			
	ALCHEMY	ALCHEMY(10K)	ZINC	ZINC(10K)
Batch Size	25	25	25	25
Learning Rate	0.001	0.001	0.001	0.001
Max Epochs	1000	1000	1000	1000
Optimizer	Adam	Adam	Adam	Adam
Scheduler	ReduceLROnPlateau	ReduceLROnPlateau	ReduceLROnPlateau	ReduceLROnPlateau
Number of 1-WL iterations	$\{1, 2, 3\}$	$\{1, 2, 3, 4\}$	$\{1, 2, 3\}$	$\{1, 2, 3, 4\}$
Use 1-WL-Convergence	False	False	False	False
MLP Activation Function	ReLU	ReLU	ReLU	ReLU
MLP Normalization	BatchNorm	BatchNorm	BatchNorm	BatchNorm
MLP Number of Layers	$\{2, 3, 4, 5\}$	$\{2, 3, 4, 5\}$	$\{2, 3, 4, 5\}$	$\{2, 3, 4, 5\}$
MLP Dropout	$X \sim U(0, 0.2)$	$X \sim U(0, 0.2)$	$X \sim U(0, 0.2)$	$X \sim U(0, 0.2)$
Embedding Dimension	{None, 16, 32, 64, 128}	{None, 16, 32, 64, 128}	{None, 16, 32, 64, 128}	{None, 16, 32, 64, 128}
Pooling function	{Max, Mean, Sum}	{Max, Mean, Sum}	{Max, Mean, Sum}	{Max, Mean, Sum}

2. Analysis

Table B.5.: Overview of the number of unique colors in the colorings computed by the 1-WL algorithm when applied to each dataset. Specifically, we specified the number of iterations of the 1-WL algorithm. Additionally, the "# Nodes" column showcases the upper bound of the number of unique colors that can be used in the colorings.

Dataset	Number of 1-WL Iterations											
	0	1	2	3	4	5	6	7	8	9	10	# Nodes
ENZYMES	2	231	10 416	15 208	16 029	16 450	16 722	16 895	17 026	17 130	17 204	19580
IMDB-BINARY	1	65	2 931	3 595	3 595	3 595	3 595	3 595	3 595	3 595	3 595	19 773
MUTAG	2	33	174	572	1 197	1 766	2 167	2 403	2 511	2 560	2 579	3 371
NCI1	2	292	4 058	22 948	44 508	58 948	68 632	75 754	81 263	85 590	88 968	122 747
PROTEINS	2	297	20 962	35 676	37 940	38 653	38 926	39 064	39 141	39 180	39 203	43 471
REDDIT-BINARY	1	566	71 893	244 529	317 728	333 258	335 961	336 412	336 490	336 506	336 507	859 254

3. Visualization of the Approximation Performance of GNNs

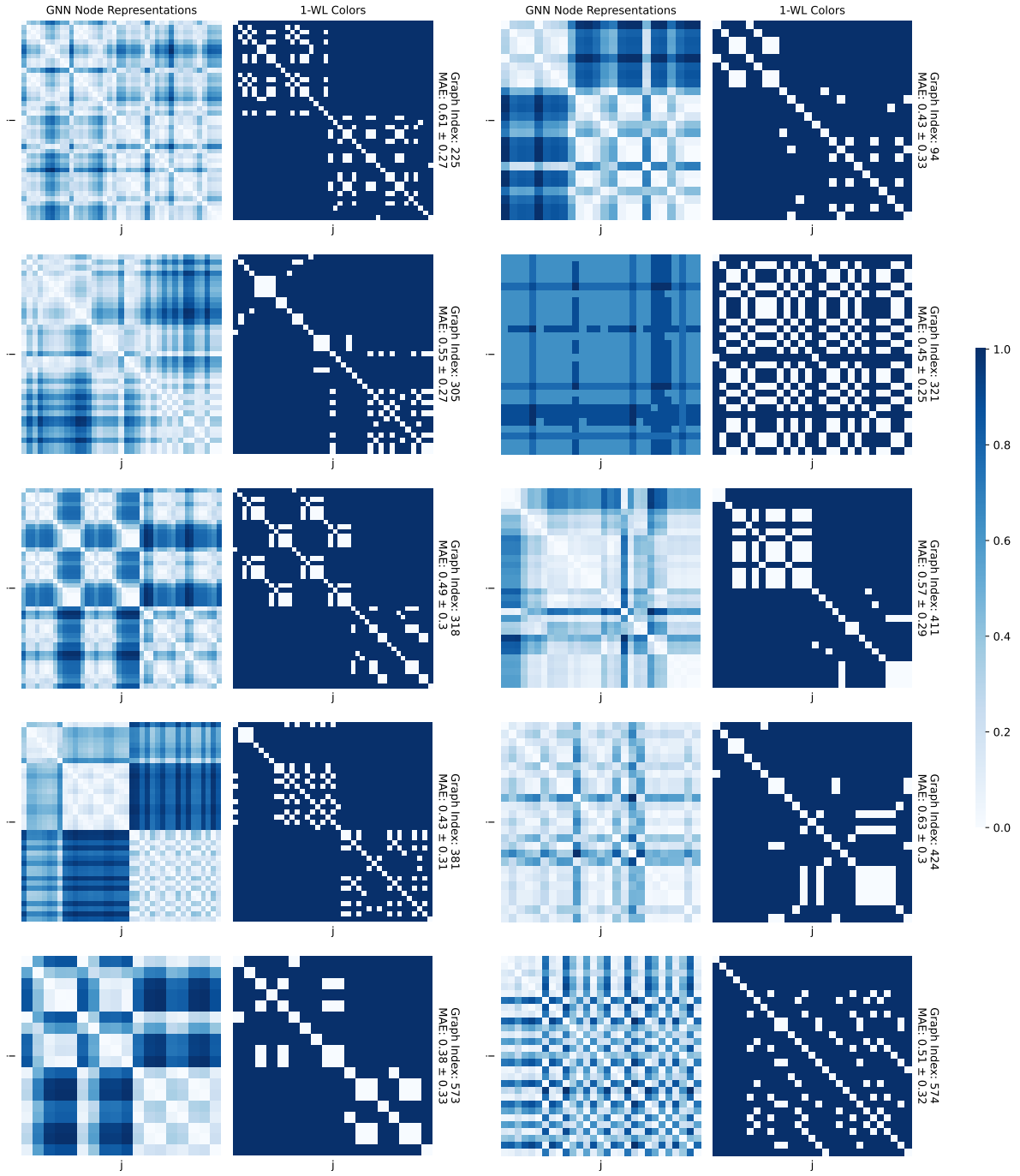

Figure B.1.: Visualizing the performance of the best performing GNN on the ENZYMES dataset in approximating node colors computed by the 1-WL algorithm. The ten graphs shown are randomly sampled from the GNN's test set, and the 1-WL algorithm ran only for one iteration. The average error for the entire test set is 0.49 ± 0.3.

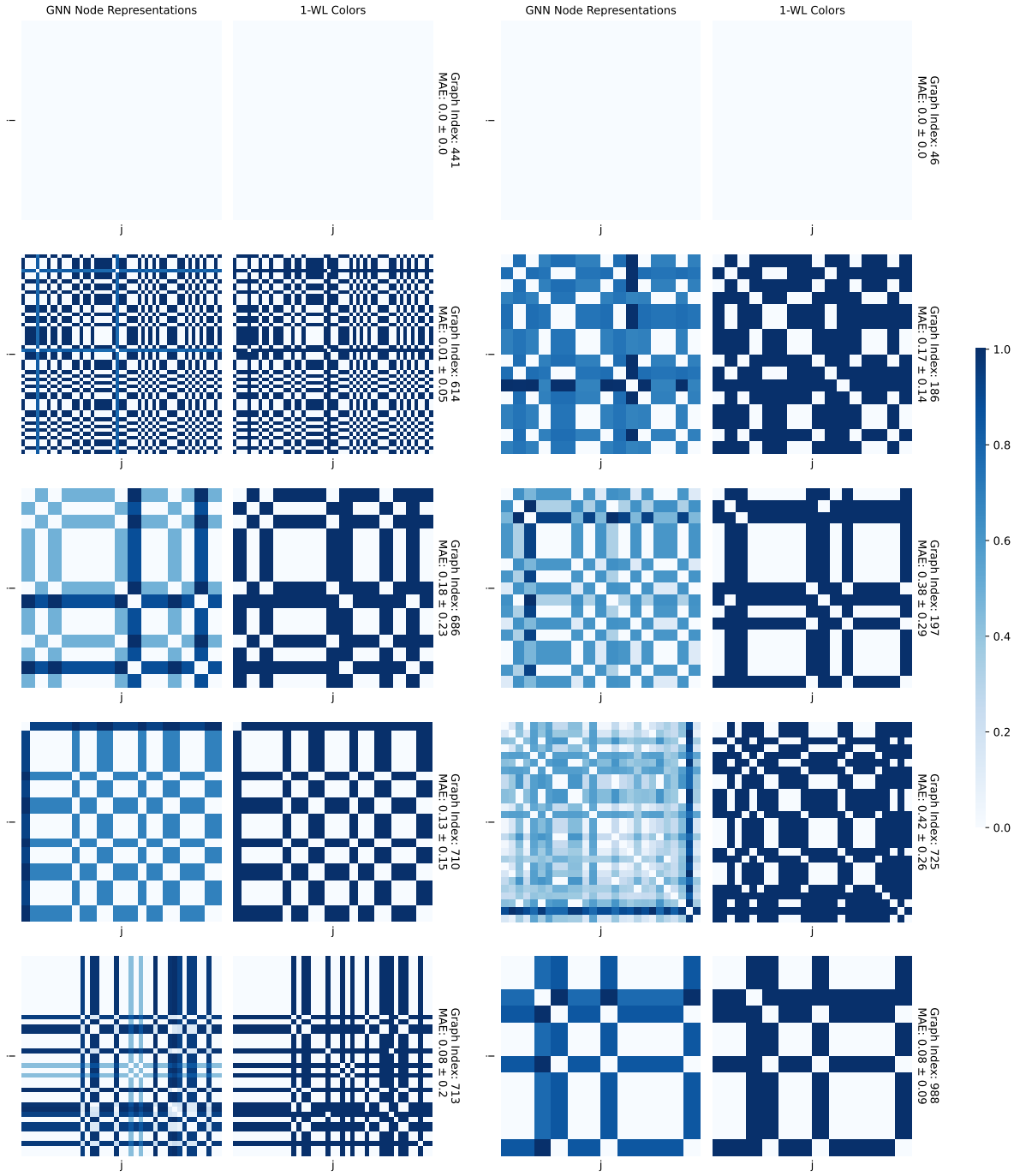

Figure B.2.: Visualizing the performance of the best performing GNN on the IMDB-BINARY dataset in approximating node colors computed by the 1-WL algorithm. The ten graphs shown are randomly sampled from the GNN's test set, and the 1-WL algorithm ran only for one iteration. The average error for the entire test set is 0.14 ± 0.15.

Note that IMDB BINARY does not contain any node features, so we artificially initialize each node feature with a one-hot encoding of its degree.

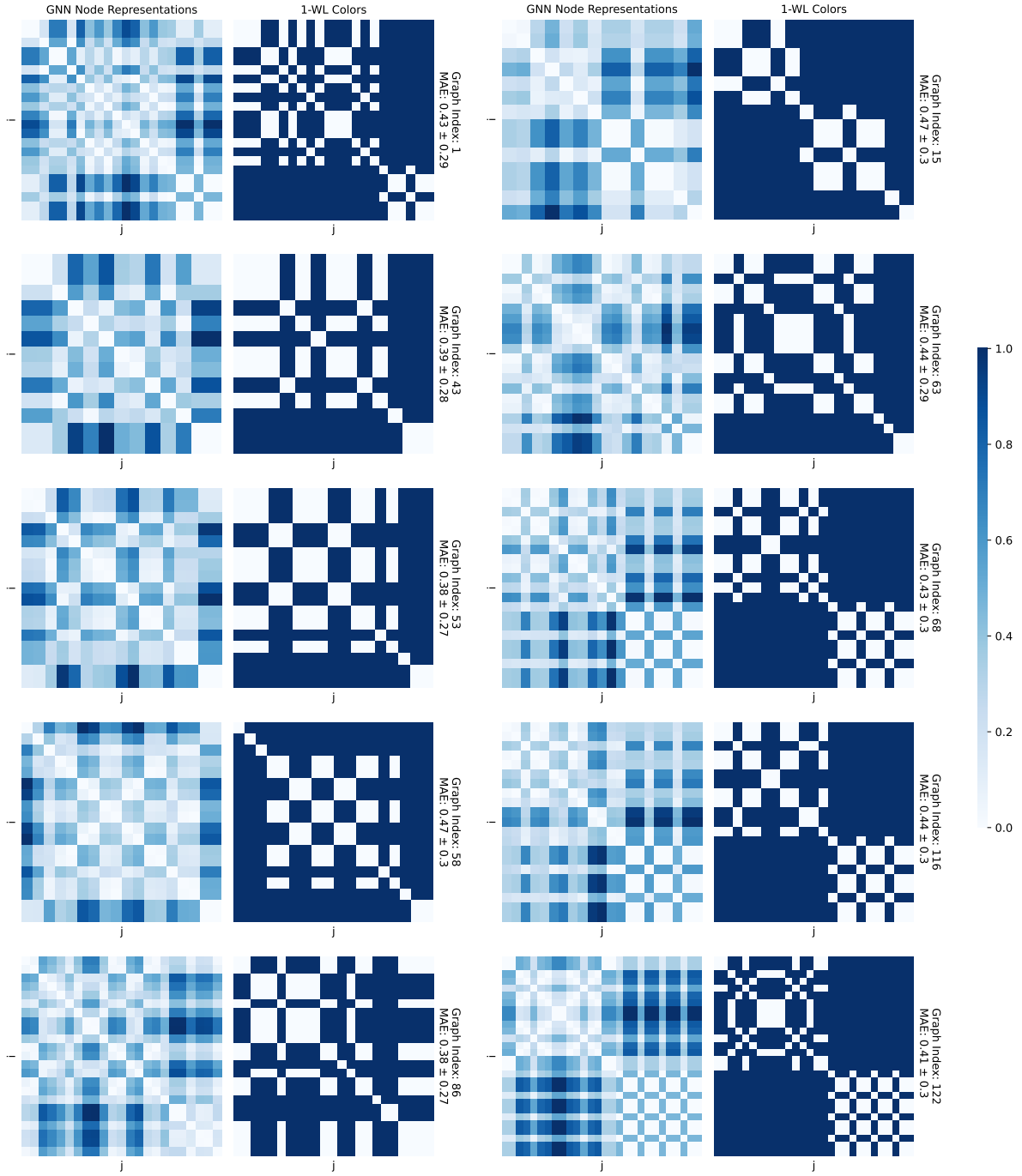

Figure B.3.: Visualizing the performance of the best performing GNN on the MUTAG dataset in approximating node colors computed by the 1-WL algorithm. The ten graphs shown are randomly sampled from the GNN's test set, and the 1-WL algorithm ran only for three iteration. The average error for the entire test set is 0.42 ± 0.29.

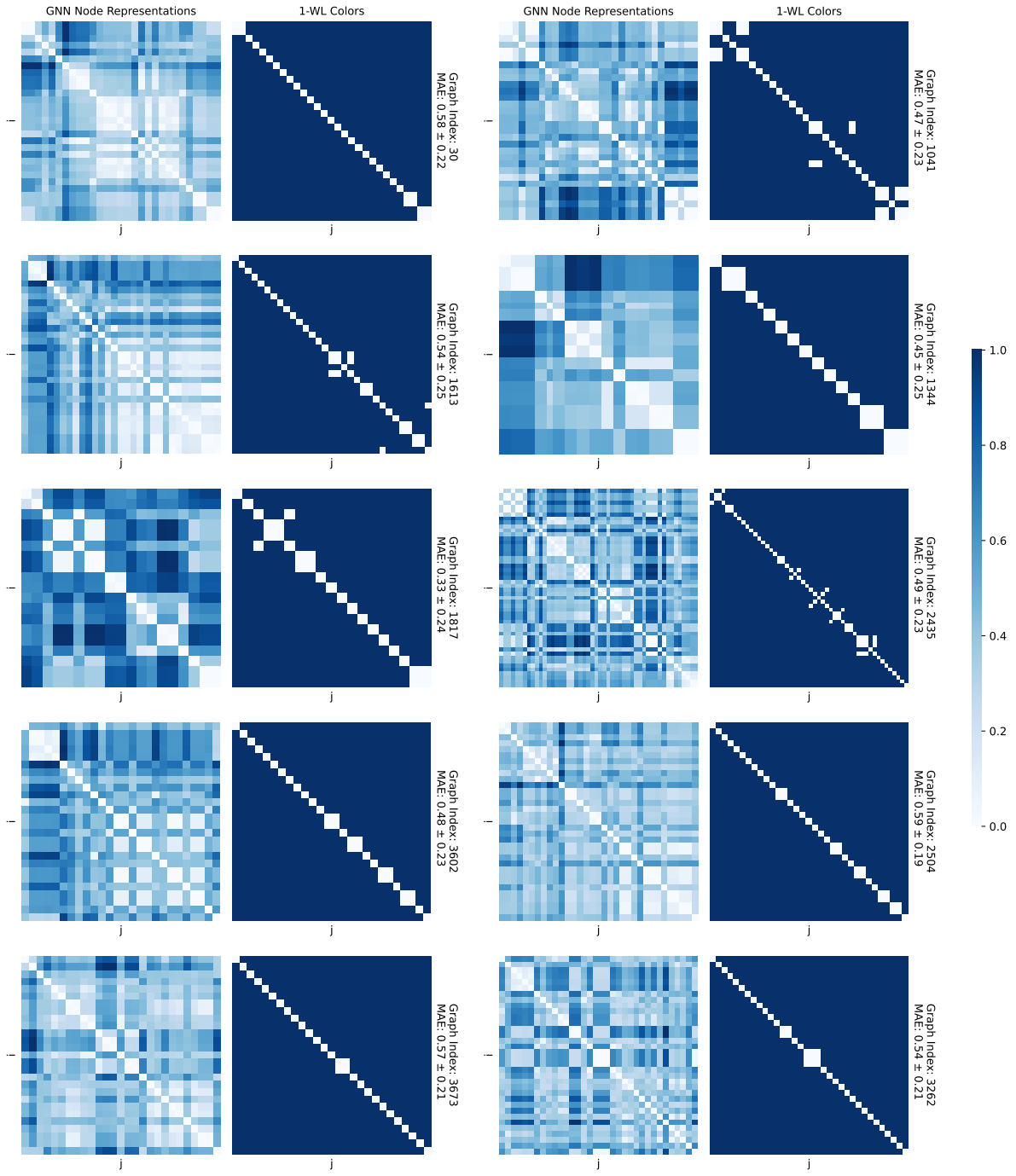

Figure B.4.: Visualizing the performance of the best performing GNN on the NCI1 dataset in approximating node colors computed by the 1-WL algorithm. The ten graphs shown are randomly sampled from the GNN's test set, and the 1-WL algorithm ran only for three iteration. The average error for the entire test set is 0.50 ± 0.24.

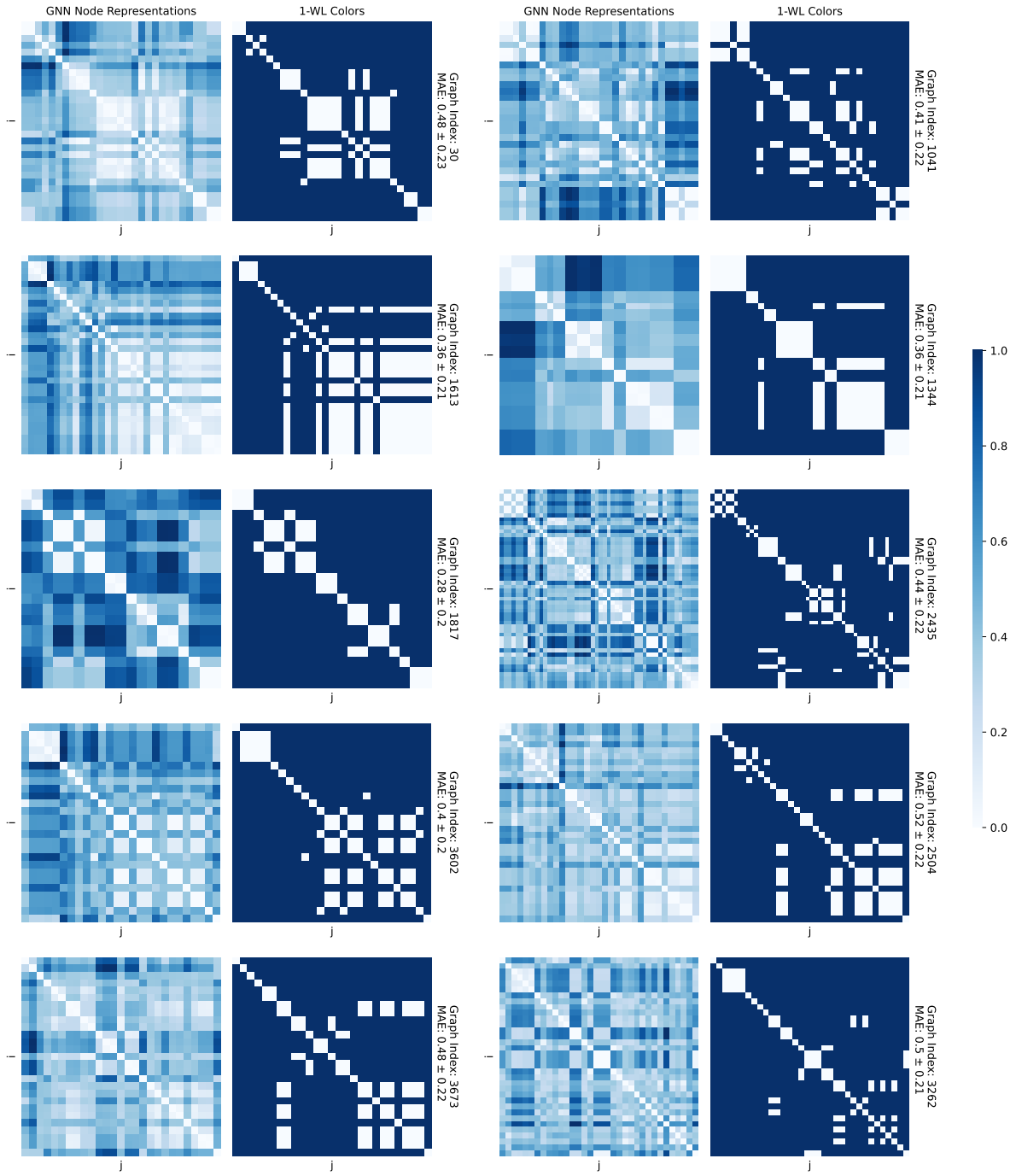

Figure B.5.: Visualizing the performance of the best performing GNN on the NCI1 dataset in approximating node colors computed by the 1-WL algorithm. The ten graphs shown are randomly sampled from the GNN's test set, and the 1-WL algorithm ran only for one iteration. The average error for the entire test set is 0.42 ± 0.22.

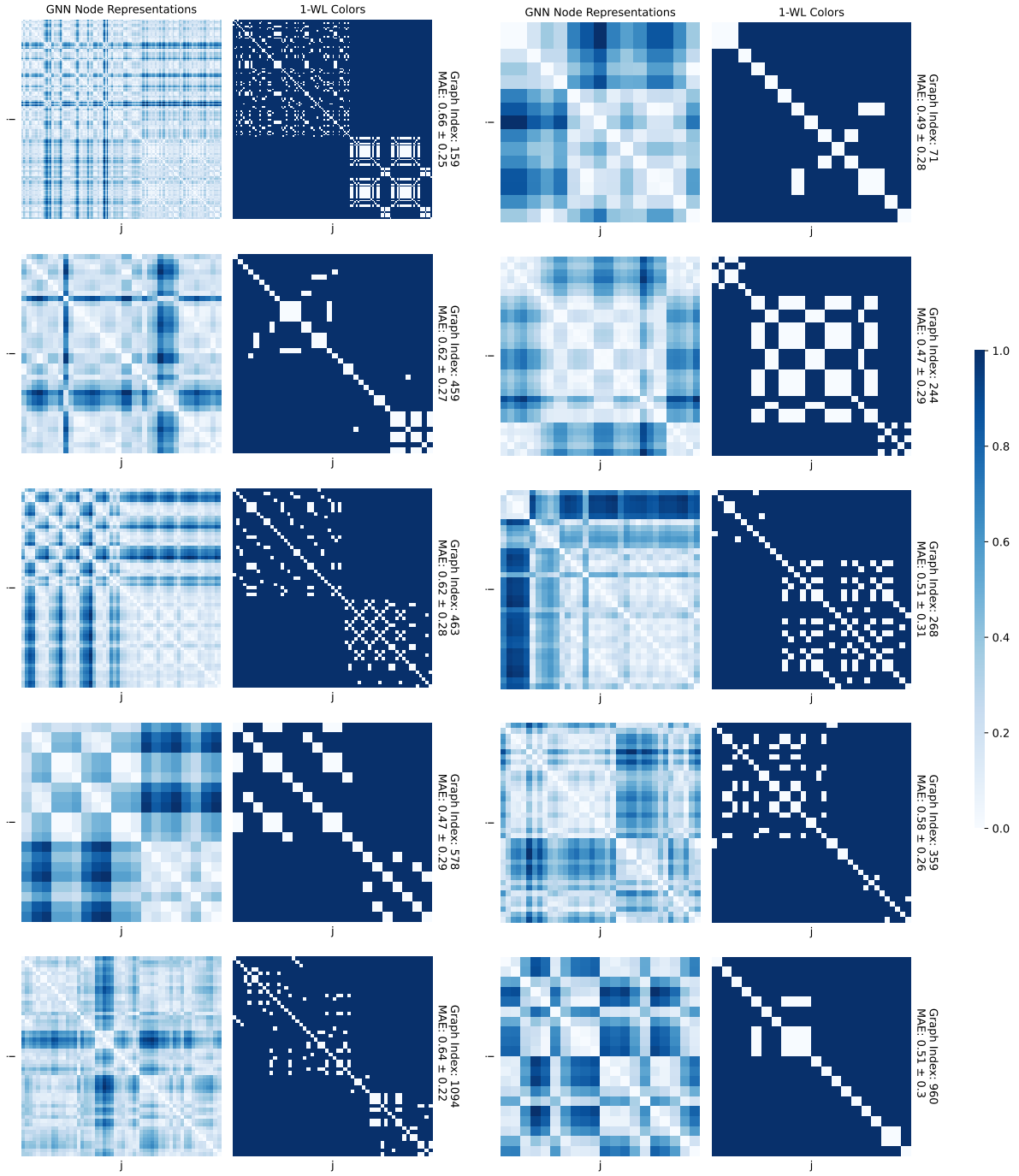

Figure B.6.: Visualizing the performance of the best performing GNN on the PROTEINS dataset in approximating node colors computed by the 1-WL algorithm. The ten graphs shown are randomly sampled from the GNN's test set, and the 1-WL algorithm ran only for one iteration. The average error for the entire test set is 0.49 ± 0.26.